

Origin, structure, and role of background EEG activity.

Part 2. Analytic phase

Walter J Freeman

Department of Molecular & Cell Biology, LSA142
University of California
Berkeley CA 94720-3200 USA
Tel. 1-510-642-4220 Fax 1-510-643-6791
drwjfiii@socrates.berkeley.edu

<http://sulcus.berkeley.edu>

Running title: Background EEG analytic phase

See: **Clinical Neurophysiology (2004) 115: 2089-2107.**

Key Words: analytic phase, basis function, phase cone, phase gradient, phase transition,
self-organized criticality, spatial EEG pattern, spontaneous cortical activity

Acknowledgments

This study was supported by grant MH 06686 from the National Institute of Mental Health, and by grants NCC 2-1244 from the National Aeronautics and Space Administration EIA-0130352 from the National Science Foundation to Robert Kozma. Programming was by Brian C. Burke. Essential contributions to surgical preparation and training of animals, data acquisition, and data analysis by John Barrie, Gyöngyi Gaál, and Linda Rogers are gratefully acknowledged.

Abstract

Objective: To explain spontaneous EEG through measurements of spatiotemporal patterns of phase among beta-gamma oscillations.

Methods: High-density 8x8 intracranial arrays were fixed over sensory cortices of rabbits. EEGs were spatially low pass filtered, temporally band pass filtered and segmented in overlapping windows stepped at 2 ms. Phase was measured with the cosine as the temporal basis function, using both Fourier and Hilbert transforms to compensate for their respective limitations. Spatial patterns in 2-D phase surfaces were measured with the geometric form of the cone as the spatial basis function.

Results: Two fundamental state variables were measured at each digitizing step in the 64 EEGs: the rate of change in phase with time (frequency) and the rate of change in phase with distance (gradient). The parameters of location, diameter, duration, and phase velocity of the cone of phase were derived from these two state variables. Parameter distributions including recurrence intervals extending into the low theta range were fractal; the mean values varied with window duration and interelectrode distance.

Conclusions: The formation of spatial amplitude patterns began with phase transitions that were documented by phase discontinuities and phase cones. The multiplicity of overlapping cones indicated that sensory neocortices maintained a scale-free state of self-organized criticality (SOC) in each hemisphere as the basis for its rapid integration of sensory input with prior learning stored in cortical synaptic webs. Further evidence came from the fractal properties of the phase parameters and the self-similarity of phase patterns in the ms/mm to m/s ranges.

Significance: These EEG data suggest that neocortical dynamics is analogous to the dynamics of self-stabilizing systems, such as a sand pile that maintains its critical angle by avalanches, and a pan of boiling water that maintains its critical temperature by bubbles that release heat. Beta-gamma oscillations stem from the ability of neocortex to maintain its stability under continuous sensory bombardment. Modeling implies that the critical parameter of neocortex (analogous to angle of repose or temperature) is the mean firing rates of neurons that are homeostatically regulated by refractory periods everywhere at all times in cortex. The advantage of SOC in perception may be the ability it gives neocortex to generate instantaneous global phase transitions (avalanches, bubbles) large enough to include the multiple sensory areas that are necessary to form Gestalts (multisensory percepts).

1. Introduction

1.1. Sudden changes in EEG occur simultaneously over large distances: phase transitions

Human perception takes place in rapid frames that engage voluminous sensory input in situations, such as a feeling about the shoulders when trying on a new coat, an understanding that a friend is angry or frightened, a flash of recognition of the identity and state of mind of a parent with one word on the telephone, and so on. Brains are usually in states of arousal and expectancy before the arrival of stimuli. These states are normally prerequisite for perception. EEG and MEG from humans and animals in such states give evidence of background spatiotemporal waves of potential that flicker ceaselessly all over the head, like the background noise of traffic, wind and surf. How might neurons create these background oscillations through interactions, and how might these waves contribute to phenomenological experiences before, during and after expected stimuli?

Recent efforts to open background activity to exploration have included recording scalp EEG with a high-density electrode array (Freeman et al., 2003) and analyzing the signals with the Hilbert transform (Freeman, Burke and Holmes, 2003). The unprecedented spatial and temporal resolution afforded by these new techniques, which were developed from research on rabbit brains, revealed remarkably detailed patterns in the seemingly featureless chaotic oscillations in electrical potential found everywhere over the scalp. Most striking was the widespread synchrony in oscillations at frequencies broadly distributed over the beta-gamma range that were aperiodically re-initialized at intervals corresponding to rates in the theta-alpha range. The distances across which the waves were synchronized varied among subjects and across samples, ranging up to 189 mm (the length of the array). Evidence was found for textures of amplitude at the scale of the gyri, 1 to 3 cm in length, indicating synchrony that extended across multiple gyri and sulci. Temporally the synchrony was interrupted but then re-established in phase jumps. Each jump lasted only a few ms and recurred at irregular intervals, yet successive jumps were nearly simultaneous, even over long distances. In subjects at rest with eyes closed the episodes of desynchronization on average were correlated with the alpha rhythm. In subjects holding their eyes open or intentionally tensing their scalp to introduce EMG, the mean repetition rate often appeared in the theta range.

A provisional explanation for these episodic patterns in scalp EEG was based on studies of spatiotemporal patterns of intracranial EEG in rabbits with high-density electrode arrays fixed surgically over the primary sensory areas (Viana Di Prisco and Freeman, 1985; Barrie, Freeman and Lenhart, 1996). The olfactory bulb and neocortical areas were found to generate spatial patterns of amplitude modulation (“AM patterns”) of oscillations in the gamma and beta ranges, respectively. The patterns lasted 80-100 ms and recurred at rates in the theta-delta range (Freeman and Barrie, 2000). Each AM pattern expressed a short-lasting state of the cortex, which formed by an abrupt change in the cortical dynamics known as a phase transition. Each phase transition had four steps. The very rapid spread of re-initialization of the phase of the beta-gamma activity (Freeman, 2001, 2004c) was followed by re-synchronization, then by the stabilization of a pattern, and an increase in amplitude of the AM pattern, all within 24-34 ms (Freeman, 2003b; Freeman and Burke, 2003; Part 1). These phase-locked spatial patterns in the EEG revealed organizations of cortical activity that were termed “wave packets” (Freeman, 1975, 2003b). Successive wave packets resembled frames in a black/white cinema with

successive spatial patterns held briefly. The AM patterns observed in sensory areas were statistically related to conditioned stimuli, not so much to the features of the stimuli as to the categories of the stimuli (Ohl, Scheich and Freeman, 2001) that provided for the meanings of the stimuli for the animals (Freeman, 2003a).

Multiple mini-arrays fixed over the visual, auditory, somatic, olfactory and entorhinal areas detected multicortical events that involved all three neocortical sensory cortices and the limbic and olfactory areas (Freeman, Gaál and Jornten, 2003; Freeman and Burke, 2003). The onsets were virtually simultaneous (Freeman and Rogers, 2003). That finding led to a search for episodic re-synchronization in scalp EEG, which might give evidence of similar widespread phase transitions in human cortex (Freeman, Burke and Holmes, 2003). The conclusion was reached that in both animals and humans the neocortex generated temporally discontinuous, broad spatial patterns that had the requisite sizes, durations, and repetition rates to qualify as candidates for Gestalts, the frames of meaning in perception (Freeman, 2003a).

In contrast to the olfactory EEG, which provided an obvious relation of bursts of activity to respiration (Freeman, 1975), visual inspection of the multichannel EEG recordings from intracranial electrode arrays on neocortex (Fig. A1.01 in Part 1) gave no clues to the temporal locations of the sequential neocortical states and the transitions by which they emerged (Barrie, Freeman and Lenhart, 1996). In both structures it appeared that responses to stimuli might take the form of abrupt re-organizations of background activity into patterns that were selected by stimuli following phase transitions that were triggered by the stimuli. Therefore, re-examination of extant data was undertaken here to answer the question, what is the neural mechanism that sustains background activity in brains and in particular gives the EEG its dynamic properties? The aperiodic oscillations for many years have been regarded as dendritic “noise” (Bullock, 1969; Elul, 1972) that is best removed by time-locked averaging of responses to stimuli (event related potentials, ERP). However, EEG has too much informative structure to be so lightly dismissed (Watters, 2000). The approach taken here to explain the “spontaneous” EEG is to measure the distributions of phase defined at frequencies in the beta-gamma range in multichannel EEG signals, and to calculate the rates of change in phase with time and distance. A companion report (Freeman, 2004, Part 1) deals with the amplitude distributions. The large data base needed for the study consisted of EEG records derived from high-density arrays implanted over sensory cortices in rabbits that were then trained to discriminate conditioned stimuli in a classical aversive paradigm (Barrie, Freeman and Lenhart, 1996).

These data were interpreted in the context of the theory of self-organization in nonlinear systems operating far from equilibrium. The term “self-organizing” means that a complex system with many interacting elements, such as an area of cortex with many synaptically interactive neurons, develops its own set of preferred states, which it constructs and modifies by changing its connections in accordance with certain rules. In the case of cortex these are the well-known rules of learning. The term “nonlinear” means that small inputs can give large outputs and vice versa; the proportionality and additivity of outputs to inputs of linear systems does not hold. Physiologists are familiar in principle with nonlinearity in terms of paired-shock testing in search of facilitation and depression, thresholds and refractory periods. Operating “far from equilibrium” means that normal cortex does not go to rest, as an isolated nerve cell does when it is deprived of input; instead, cortex continually boils with background activity that requires

metabolic energy that is supported by a steady supply of oxygen and glucose and removal of waste heat and carbon dioxide.

EEG background activity, which is not truly “spontaneous”, has several statistical properties that are characteristic of self-organizing systems; they are fractal, scale-free, and self-similar. The distributions of the sizes and durations of events are fractal (Mandelbrot, 1983), not normal. Whereas events in normal distributions have means and standard deviations that are independent of the dimensions of the tools of measurement, events in fractal distributions have means that tend to be equal to the standard deviations, and both mean and standard deviation (SD) decrease with decreasing size of the measuring tool. Systems that are characterized by fractal distributions of their properties are called and “scale-free” (Wang and Chen, 2003). The classic example is the length of the coastline of England, which varies with the size of the measuring stick from kilometers to microns. In histograms the distributions are not bell-shaped but have maximal numbers at minimal dimensions. Small, brief structures and events have the same appearance and proportions as large, long-lasting events. This property is called “self-similarity”. It is often applied to anatomical structures such as dendrites, in which branchlets far from the cell body have the same appearance as branches close in. The spectra of EEG signals often show the $1/f$ power-law distribution across frequencies (Freeman et al., 2003), which is an example of self-similarity (Pereda et al., 1998; Watters, 2000; Hwa and Ferree, 2002). The self-similarity of events in a scale-free network offers a key to understanding how cortical gamma synchronization can be reinitialized by a phase transition over much of a human cerebral hemisphere (Cover Illustration, Fig. A1.12 in Part 1) without impediment by sulci in under a quarter cycle duration of a gamma wave (Freeman, Burke and Holmes, 2003). This time frame is as rapid as the re-set of phase over the much smaller rabbit olfactory bulb (Freeman and Baird, 1987).

All these properties point to a special kind of self-organization, which is termed self-organized criticality (“SOC”, Bak, 1996; Jensen, 1998). The structural properties of axons and dendrites have already been shown to be fractal (Braitenberg and Schüz, 1991). If the distributions of the spatial and temporal measurements of the EEG data can be shown to be fractal, then the basis for relations between the animal and human EEG may become apparent through self-similarity (Cover Illustration). Most importantly, SOC might explain how human cerebral hemispheres can reorganize their activity patterns almost instantly over distances that can exceed the dimensions of most dendritic arbors by two to three orders of magnitude and perhaps thereby “bind” (von der Malsburg, 1983) the sensory information that is held transiently in multiple widely dispersed areas almost instantly into Gestalts.

2. Methods

2.1. *Experimental animals and EEG recording*

A cursory description has been given in the preceding report, Part 1, of the methods by which the EEG data were acquired from rabbits that were conditioned to discriminate visual, auditory, or somatic conditioned stimuli in a classical aversive paradigm. EEG signals were recorded from high-density 8x8 epidural arrays over one of the three cortices in each of 2 rabbits totaling 6 sessions. Electrode spacing averaged 0.79 mm giving an array window of 5.6x5.6 mm. Sampling after analog filtering at 0.1-100 Hz was at 500 Hz by 12-bit ADC after multiplexing at 10 microsecond/channel. Blocks of data were stored in 6-s trials including 20 trials with a reinforced CS+ and 20 trials with a CS- not reinforced. Analysis was done off-line on a Macintosh platform with MATLAB software.

2.2. *Methods for measuring frequency and phase gradient: temporal basis functions*

Measurement of EEG requires selection of elementary waves and geometric shapes called “basis functions” (Freeman, 1975). Basis functions are adjusted and added like weights on a scale until their sum matches the wave pattern to be measured, which is then said to be “decomposed” into its numbered parts. In the time domain the most widely used basis function is the sinusoidal wave of oscillation at one frequency, phase and amplitude. When the wave is started with maximal amplitude at time zero lag, it is called a “cosine”. For simplicity, that is the basis function adopted here to get the Fourier phase, $\phi_1(t)$ (Appendix 2.1). Other options that have been used with these data have been Fourier decomposition by the FFT to get a range of cosines in the temporal spectrum (Appendix 1.1, Part 1) followed by selecting the phase at the frequency having the greatest power (Barrie, Freeman and Lenhart, 1996); decomposition with nonlinear wavelets that allow the frequency and amplitude to vary with time (Freeman and Viana Di Prisco, 1986, Freeman, 2003b); and digitizing, in which the basis function is a rectangular wave with the variables of pulse height and latency, in order to decompose a waveform into a sequence of rectangular waves at the sample interval. This basis function is the key to using the Hilbert transform.

For application of any or all of these temporal basis functions to measure EEG waves, the next step is to select an optimal temporal band pass filter. In prior studies the ultimate criterion for choosing the upper and lower cut-off frequencies was optimization of the classification of spatial patterns of amplitude modulation of brief epochs of gamma oscillations (AM patterns) with respect to conditioned stimuli (CS) (Freeman and Viana Di Prisco, 1986; Freeman and Grajski, 1987; Barrie, Freeman and Lenhart, 1996; Ohl, Scheich and Freeman, 2001; Freeman, Gaál and Jornten, 2003; Freeman and Burke, 2003). The proximate criterion for optimization of the pass band was to cross-correlate the unfiltered EEG with the unfiltered analytic phase differences on each channel, calculate the cospectrum (Fig. A2.03 and Fig. A2.07, D), find the frequency at which power in the alpha band was maximal, and measure that power (Fig. A1.02, A in Appendix 1.1, Part 1). Next the low-pass cut-off was applied at a frequency varied in steps from 80 Hz down to 12 Hz to construct a tuning curve (Freeman, Burke and Holmes, 2003). The cut-off frequency giving the highest power in the alpha range was fixed, and the high-pass cut-off was applied in steps from 4 to 20 Hz to construct a second tuning curve and find the maximal

power. These tuning curves gave the optimal pass band for use of the Hilbert transform (Appendix 1.3, Part 1).

Use of temporal basis functions also required segmentation of the EEG signals. The minimal duration for the Fourier window was the wavelength of the high pass temporal filter. The maximal duration could not exceed the intervals between successive phase transitions, which served to define periods of “stationarity” in the EEG, meaning that the cortex was maintaining a defined state with constant statistical properties between transitions (Freeman, 2000). The minimal duration for the Hilbert window was the digitizing interval, and the maximal duration could not exceed the wavelength of the average frequency within the window, owing to the branch points imposed on calculation of analytic phase by the arctangent (Appendix 1.3, Part 1). The desired parameters in each window of the multichannel recordings were the frequency in Hz common to all channels, which multiplied by 2π equaled the temporal phase gradient in rad/s, and the phase on each channel at that frequency with respect to the phase of the spatial ensemble average waveform, from which spatial phase gradient was calculated in rad/mm (Appendix 2.2).

2.3. Justification of the choice of the phase cone as the spatial basis function

In the 2-dimensional spatial domain the simplest options for the basis functions to measure the phase gradient were a plane, a radially symmetric bivariate Gaussian density function, or a circular cone (Freeman and Baird, 1987). Each basis function was fitted to the phase data by nonlinear regression with the criterion of minimizing least squares residuals (Appendix 2.2). Preliminary results from fitting the same olfactory test data with all three basis functions (Freeman and Baird, 1987) showed that the cone gave the smallest % residuals and the simplest interpretation of phase velocity as an expression of axonal conduction velocity in m/s (see equation 4 in Section 2.4). All of these simple basis functions had the drawback that most 8x8 matrices of numbers could be fitted, whether or not they had structure, giving parameters that might indicate structure where none existed. Stringent statistical controls with data randomization were needed (Appendix 2.3). The additional requirements were imposed that a stable cone persist over time in respect to the location and sign of its apex, and that the residuals from cone fitting be less than 30% of the total variance of the 8x8 phase surface (Freeman and Barrie, 2000; Freeman, 2003b). The measurement of phase was greatly facilitated by low pass spatial filtering (Fig. A2.04), for which the criterion was the concave-upward inflection in the spatial PSD_x at high frequency (Fig. A1.02, B, Appendix 1.2, Part 1, Freeman and Baird, 1987; Barrie, Freeman and Lenhart, 1996). Spatial filtering imposed structure on the data from the 8x8 arrays, so that care had to be taken to study by use of randomized controls the degree to which structuring occurred (Appendix 2.3).

Validation of choosing the cone as the spatial basis function came from comparing the results of measurement with known anatomical, physiological and behavioral properties of the EEG. Measurements of the gradient of the cone gave estimates of the phase velocity that fell within the known range of conduction velocities of axons running parallel to the pia (reviewed in Freeman and Barrie, 2000). Connectivity of individual neurons in neocortical neuropil is sufficiently low (Braitenberg and Schüz, 1991) that the neurons are not dragged into zero-lag synchrony within the duration of a phase cone; the radial lag in phase transition is preserved in the cone. Estimates of the cone diameters were large enough to encompass multiple domains in each primary sensory

area for perceptual integration (“feature binding”, von der Malsburg, 1983; Singer and Gray, 1995) but small enough to fit within the brain. An electrophysiological criterion was to demonstrate a peak in the alpha or theta range of the cospectrum of the cross-correlation function between a sequence of cones and the spatial ensemble average of the unfiltered EEG (Freeman and Barrie, 2000; Freeman and Rogers, 2002), which was used for optimizing the pass band prior to use of the Hilbert transform. Identifying stable phase cones and using them to locate AM patterns improved the classification rate with respect to CSs (Freeman and Barrie, 2000; Freeman, 2003b), showing that phase cones were relevant to behavior.

2.4. Theoretical validation of using the phase cone as a spatial basis function

From the standpoint of modeling, the cone is significant as a potential marker for the occurrence of phase transitions in cortical dynamics (Freeman, 2000, 2003a). In a distributed system a phase transition is unlikely to occur everywhere at the same instant. It begins at one point called a site of nucleation and spreads radially across the system (Freeman, 1990), just as a snowflake or a raindrop enlarges with radial symmetry. When a new cortical state appears that is expressed in a shared oscillatory waveform, the delay in onset imposes a radially symmetric gradient in the phase that is defined at the peak frequency of the dominant component. With multiple frequencies there are multiple phase cones that overlap in time and space in all neocortical areas studied (Freeman and Barrie, 2000; Freeman, 2003b), but not in the prepyriform cortex (Freeman and Barrie, 2000) where there are no cones, or the olfactory bulb where there is only one cone at a time with a different phase gradient in rad/s for each frequency but the same phase velocity in m/s for all frequencies (Freeman and Baird, 1987). Owing to the variability of cone parameters, measurement of a large number of phase cones was needed to evaluate and classify the distributions in histograms of the parameters. Both the Fourier and Hilbert transforms were used to measure phase in order to replicate the measurements where the techniques overlapped, to complement the limitations of each method, and benefit from the unique strengths of each.

2.5. Methods for parameterization of stable phase cones

Statistical summaries were computed of the data from each subject of the basic parameters of temporal and spatial wavelengths for each cone (for symbols see Table 1.1 in Freeman, Part1):

$$\text{Temporal wavelength, } W_t = 1000/(2\pi f_i) \text{ ms/rad} \quad (1)$$

This was simply the reciprocal of the frequency measured in Hz and converted to radians/ms (Appendix 2.1).

$$\text{Spatial length, } W_x = 1 / |\gamma_k| \text{ mm/rad} \quad (2)$$

This was simply the reciprocal of the absolute value of the phase gradient measured in radians/mm (Appendix 2.2). These two basic parameters gave two physiological parameters for each cone:

$$\text{Diameter, } D_x = (\pi/2) W_x \text{ mm} \quad (3)$$

Each cortical state formed by a phase transition had phase differences that increased with distance in all directions from the site of nucleation at the apex of the cone. The strength of synaptic interactions was assumed to be weakened by the phase dispersion. Demonstrably the spatial coherence fell to lower levels with increasing distances between recording sites. A soft boundary condition was identified as the half-power radius at which the cosine of the phase difference fell to 0.7 ($\pi/4$ radians = 45°).

$$\text{Phase velocity, } \beta = 2\pi f_i / \gamma_k = W_x / W_t \quad \text{m/s} \quad (4)$$

Simply put, long spatial wavelengths (large W_x) and high temporal frequencies (low W_t) required high velocities. Alternatively stated, at any given frequency, f_i , the flatter was the phase gradient, γ_k , the faster must have been the speed of propagation, β .

Persisting phase cones characterized as “stable” were identified by scanning the cone fits at successive steps of the moving window in accordance with the following criteria: no change in sign of gradient, γ_k , no shift of frequency, f_i , outside the temporal pass band, no shift of the apex by a step exceeding the interelectrode distance, 0.79 mm, and no location of the apex beyond twice the spatial dimensions of the array (Freeman and Barrie, 2000). The duration was given by the window length plus the number of digitizing steps for which the criteria were met times the digitizing interval (2 ms). The recurrence interval was the time lapse between successive starting points of cones meeting the criteria. After initial compilation the solutions were screened again while applying the following additional criteria for qualification: % residuals of cosine fit <20%; % residuals of cone fit <30; and no value of γ_k within the standard error of measurement ($-.04 \text{ rad/mm} < \gamma_k < .04 \text{ rad/mm}$ in Freeman and Viana Di Prisco, 1986). The % residuals criteria were adopted from prior studies of these data using FFT decomposition (Freeman and Barrie, 2000) or wavelet decomposition (Freeman, 2003b), which had been validated by optimizing the behavioral correlation of AM patterns with CS. Re-evaluation here showed that the prior criteria were appropriate for evaluating the parameters of phase cones by both Fourier and Hilbert methods.

2.6. Three methods for randomizing the EEG in space, time, or both space and time

Controls were instituted by modifying the 64 EEGs before spatial and temporal filtering. The spatial control was by randomizing the channel order with a table of random numbers. The temporal control was from surrogate data obtained by taking the FFT, randomizing the phase values, and taking the inverse FFT. Randomizing in both temporal and spatial domains simultaneously was by shuffling each of the 64 traces. A time point was selected at random in each signal, and the data after that point were moved as a block and placed in front of the remaining segment (Appendix 2.3).

3. Results

3.1. Measurement of phase gradients with the Fourier method

Reliable convergence of nonlinear regression in fitting the cosine basis function to the EEG segments (Appendix 2.1) was enabled by preprocessing: editing, temporal band pass filtering (Appendix 1.1, Part 1) preceded by spatial low pass filtering (Appendix 1.2, Part 1), and segmentation in short, medium and long window durations. Each overlapping window stepped at 2 ms yielded 2 phase surfaces expressed in 8x8 matrices. Detailed analysis was undertaken of the phase surface incorporating the larger fraction of the total variance. Each matrix representing the dominant phase surface in a window was fitted with a conic basis function (Appendix 2.2). Convergence of nonlinear regression in 2-D was achieved in 96% of windows. Two examples from visual cortex are shown in Fig. 2.01, A and B, with the fitted cones (C and D) and the residuals (E and F). Randomly about half of the apices were upward (phase lead with a positive gradient = “explosion”) and half were downward (phase lag with a negative gradient = “implosion”). Stable cones were identified by 4 criteria (Fig. 2.02, A): the frequency given by regression was within the temporal pass band; the apex of the cone was within a distance (B) less than twice the mean radius of the array from its center; the location of the apex remained within a distance (C) equal to the interelectrode interval (.79 mm) for at least two successive windows; the sign of the apex (lead or lag) did not change. After initial compilation the solutions were screened again with the following additional criteria for acceptance: % residuals of cosine fitting <20%, % residuals of cone fitting <30% (frame D). These 2 criteria were adopted from prior studies after re-evaluation on the basis of the effects of randomization of the EEG before curve fitting (Appendix 2.3) supported them.

One further requirement was imposed that no absolute value of the phase gradient, $|y_k|$, be less than 0.04 rad/mm, which was less than the standard error of phase measurement (Freeman and Viana Di Prisco, 1986). This criterion removed about 2.5% of the gradients as outliers for which the diameter, D_x , exceeded by equation (3) the length and breadth of the rabbit forebrain, ~40 mm, and most estimates of velocities, β , by equation (4) that exceeded 10 m/s. The cones qualifying as stable were identified by their conformance to all of the criteria (Fig. 2.2, A). Each criterion was imposed without the others, so there was no dependence on order.

The locations of the apices prior to imposing the criteria were scattered over the face of the array and in the surround (Fig. A2.02), usually with clumping, and often with segregation of those with lead (+) from those with lag (o). The scatter became sparse when the criteria were imposed with less clumping near the array center but with persisting segregation. The qualifying cones were treated as a time series for display in a sequence of bars indicating the number of sequential steps that each stable cone persisted (Fig. A2.03, A). The window duration had to be added to these steps to get the full duration of each phase cone, but that was omitted from the display because of the overlap, often of 4 to 6 cones at the same time, unlike the olfactory bulb that had only one cone at a time (Freeman and Baird, 1987). The PSD_T was calculated (Fig. A2.3, C) of the autocorrelation of the segments (shown in a 250 ms frame in A) representing the phase cones over the 2000 bins (4 s period of analysis). The PSD_T was also calculated (Fig. A2.3, B) of autocorrelation function of the spatial ensemble average of the unfiltered EEG. The PSD_T of the cross-correlation of the qualifying cone series with the EEG usually showed a peak in the theta range (D). The maximal power was most often in the delta range.

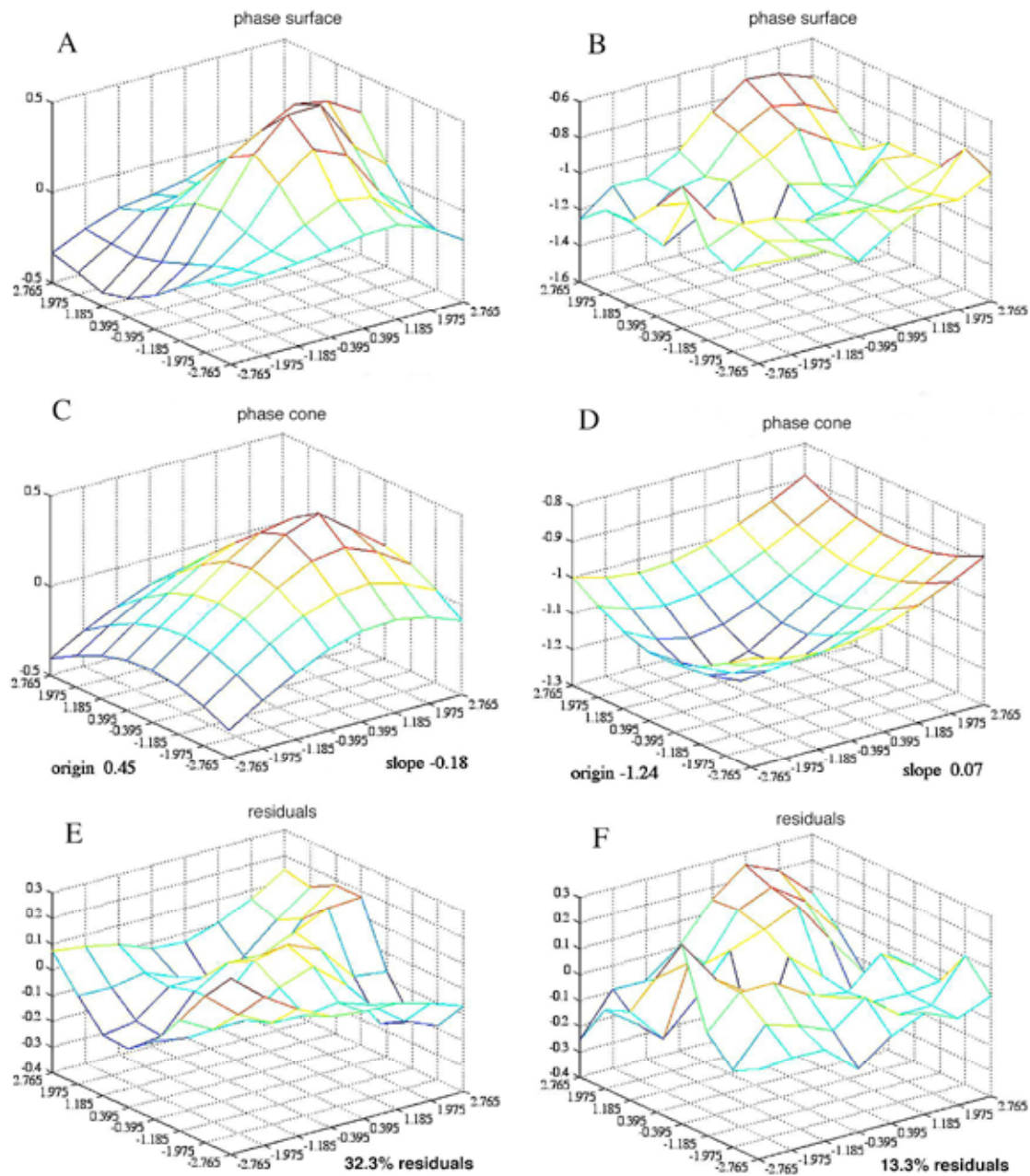


Fig. 2.01. A, B. Two examples are shown of phase surfaces, ϕ_1 , from the same trial at different times. C. The fitted upright cone, Φ , has maximal phase lead at the apex ('explosion'). D. The fitted inverted cone has maximal lag at the apex ('implosion'). E, F. Residuals from spatial fitting (Appendix 2.2).

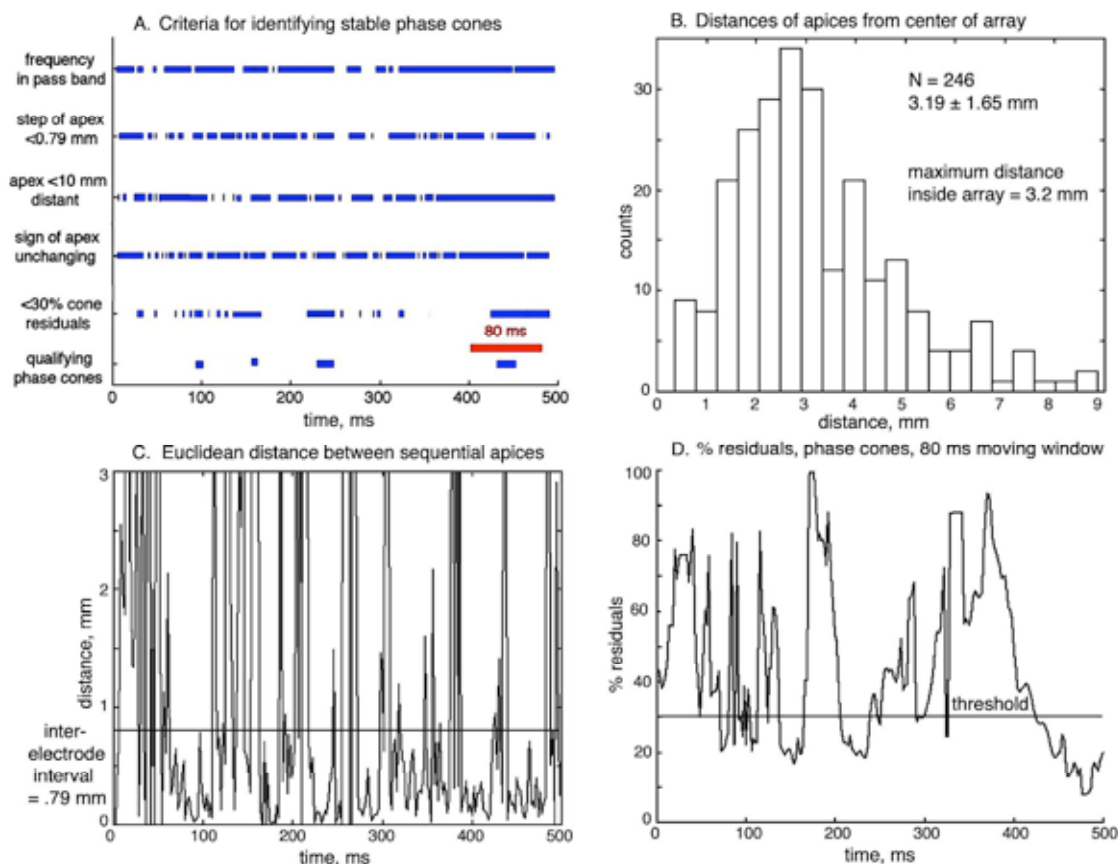


Fig. 2.02. A. The bars show the times in a 500 ms segment when each criterion was met. The overlap of these bars gave the qualifying cones. The bars indicate the number of steps to be added to the window shown by the 80 ms inset bar. **B.** As expected, the numbers of apices increased with distance from the center of the array to the edge and then fell rapidly outside the array. **C.** The distances of serial steps within stable cones were far less than those between successive stable cones. **D.** The % residuals fluctuated widely as the window was moved along the time series.

3.2. Calculation of the parameters of phase cones

The two measured quantities in each frame were the phase gradient with time (frequency f in Fig. 2.03, A and C) and the phase gradient with distance (slope of the cone β in Fig. 2.04, A and C). To normalize their distributions for statistical comparisons they were expressed as temporal wavelength W_t (Fig. 2.03, B and D) and log spatial wavelength W_x (Fig. 2.04, B and D). Summary values are given in Table 2.1. The distributions of frequencies, f_k , conformed to the spectral pattern within the boundaries imposed by the temporal band pass filter (Fig. 2.03, A and C). Conversion to temporal wavelength, W_t , by equation (1) flattened the distribution (B and D). The distributions of phase gradients were bimodal (Fig. 2.04, A and B). On average across all sets about half had phase lead ('explosion') and half had phase lag ('implosion'). Distributions from the two sets from visual cortex were biased toward phase lead (A), and those from somatic cortex more often had phase lag (C), those from auditory cortex were more symmetric. The absolute spatial wavelengths, W_x , by equation (2) were strongly skewed to shorter values; the

form of the histograms of $\log W_x$ approached the normal density function (B and D). Zero correlation was consistently found between the two gradients in the temporal and spatial dimensions (Fig. A2.05).

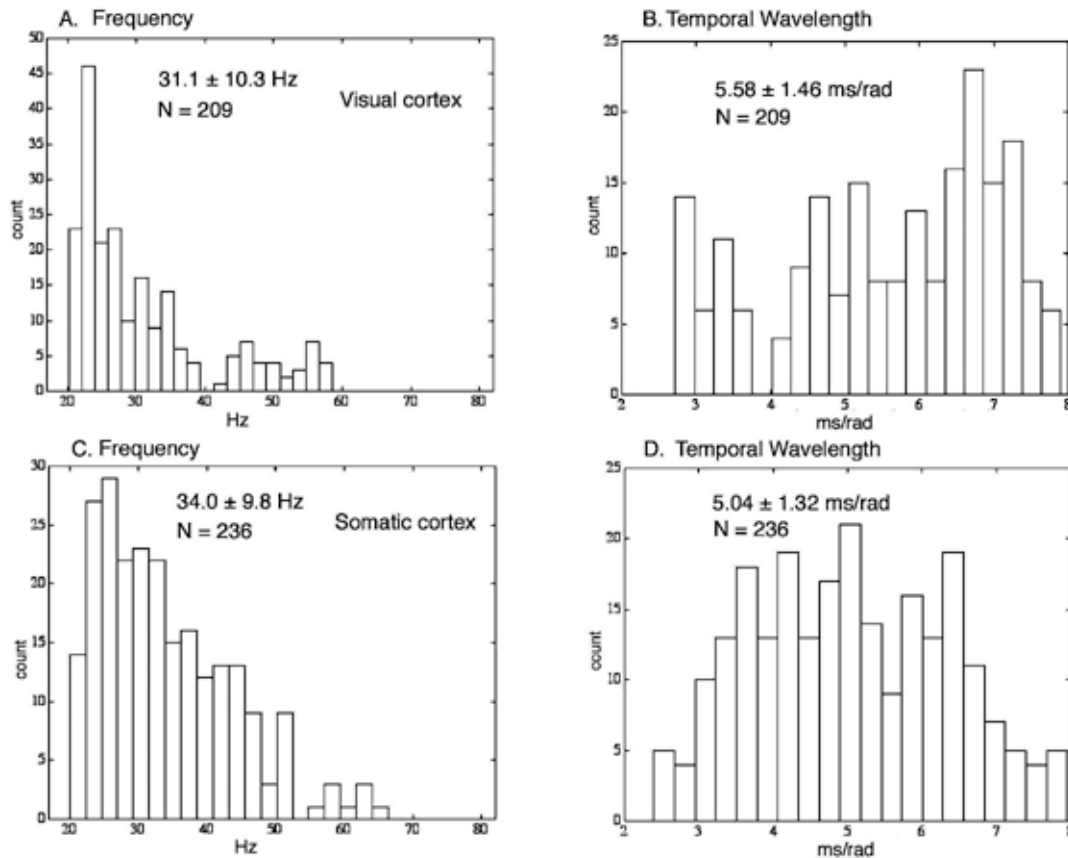


Fig. 2.03. A, C. The distribution of frequencies of the dominant cosine, f_k , mimicked the $1/f^\alpha$ form of the PSD. B, D. The temporal wavelengths, W_t , derived by equation (1) gave relatively flat distributions, often tending toward Gaussian, enabling statistical comparisons. The visual cortex tended to give lower frequencies and longer wavelengths than the somatic cortex, but the differences were not statistically significant.

One of two main physiological parameters desired from the wavelengths was the phase velocity at which the domains of spatial coherence were established, so that the relation to axonal conduction velocities and distances might be examined (Fig. A2.06, A and C). The histograms of the phase velocities from equation (4) were bimodal and skewed in accordance with the gradients. Low values were unbounded. High values were bounded by the limits on resolution of phase in nearly flat gradients. The other main parameter was the diameter of the domains as measured by the distance at which the shared power fell to one half owing to the progressive phase dispersion (B and D). Few diameters were found <5 mm, due in part to the spatial filter at 0.32 c/cm (3 mm wave length) but more to volume conduction that attenuated high spatial frequencies of dendritic potentials recorded at the pial surface. The few diameters >40 mm were rejected as exceeding brain size. Summary statistics are given in Table 2.2. The mean values

differed between sets 2-3 fold, but the SD were half or more of the means. There were too few sets from the 3 cortices (each contributed by 2 of the 6 rabbits) to judge the statistical significance of intercortical differences. Phase velocity and diameter were strongly correlated with each other but not with frequency. Durations were estimated from the number of digitizing steps over which the qualifying cones were stable plus the window duration (Fig. 2.02, A). The intervals were measured between starting points. Both were strongly dependent on the window length (see Section 3.4).

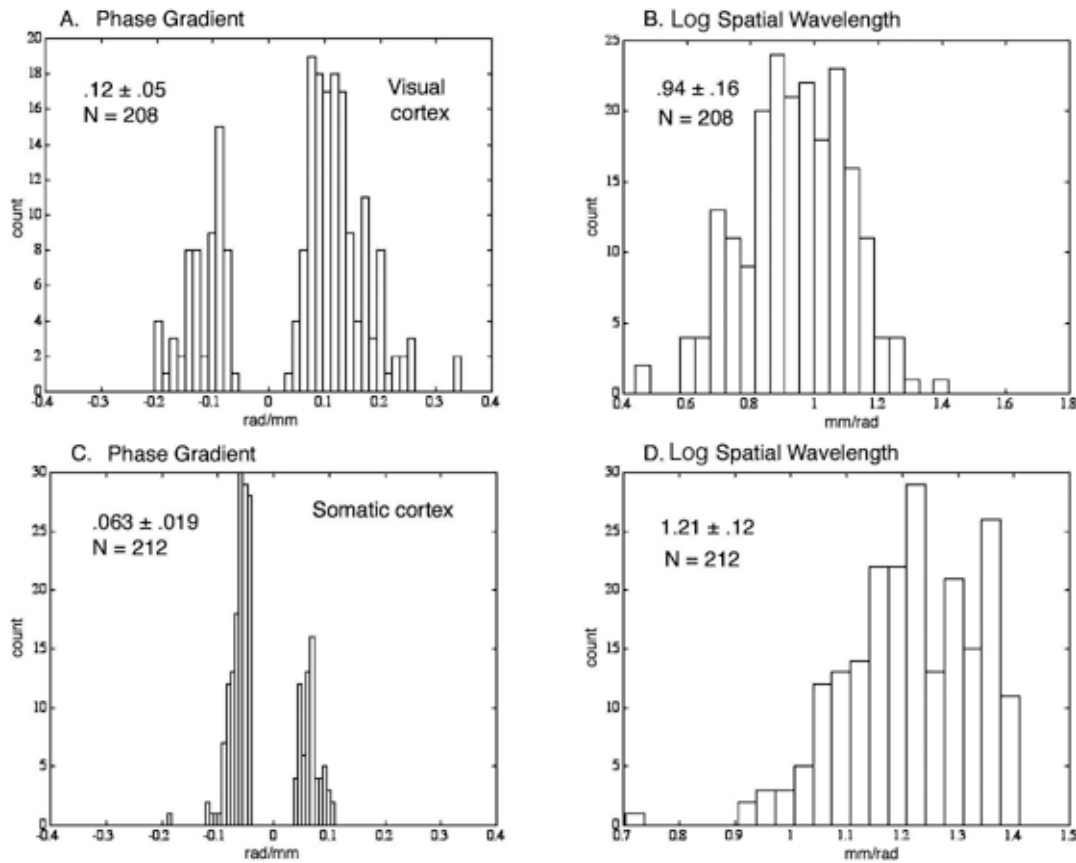


Fig. 2.04. A, C. The distributions of gradients, γ_k , were bimodal, usually asymmetric as shown, but with equal numbers on average. **B, D.** Log spatial wavelengths, W_x , calculated from the absolute values of gradients with equation (2) gave nearly Gaussian distributions.

Table 2.1. Mean \pm SD of phase parameters: FFT/Hilbert

subject	N/s	frequency Hz	gradient rad/mm	W_t ms/rad	W_x mm/rad
Visual152	12.3	28.2 \pm 6.1	.126 \pm .073	5.90 \pm 1.20	8.3 \pm 3.2
HT	14.2	33.7 \pm 7.6	.188 \pm .085	4.95 \pm 1.04	5.86 \pm 2.1
Visual9520	9.6	26.9 \pm 6.6	.172 \pm .078	6.18 \pm 1.14	7.3 \pm 3.7
HT	12.0	33.6 \pm 7.2	.219 \pm .096	4.96 \pm 1.05	5.02 \pm 1.8
Auditory531	4.1	34.6 \pm 10.1	.063 \pm .019	4.98 \pm 1.35	16.9 \pm 4.2
HT	9.8	39.8 \pm 10.2	.095 \pm .051	4.29 \pm 1.18	11.8 \pm 4.3
Auditory553	13.0	31.1 \pm 10.3	.123 \pm .050	5.59 \pm 1.46	9.4 \pm 3.5
HT	28.8	39.0 \pm 10.2	.182 \pm .085	4.37 \pm 1.16	6.07 \pm 2.2
Somatic592	7.5	39.6 \pm 14.6	.109 \pm .040	4.56 \pm 1.59	10.5 \pm 4.0
HT	49.7	42.7 \pm 10.4	.151 \pm .068	3.97 \pm 1.06	7.24 \pm 2.4
Somatic220	14.9	35.7 \pm 12.4	.073 \pm .025	4.94 \pm 1.50	15.2 \pm 4.7
HT	80.1	43.7 \pm 11.3	.112 \pm .058	3.91 \pm 1.12	10.0 \pm 3.7
Mean FFT	10.2	32.7 \pm 4.8	.111 \pm .040 ^b	5.36 \pm 1.38	11.4 \pm 4.1
Mean HT	32.4	38.8 \pm 4.3	.158 \pm .048 ^b	4.41 \pm 0.46	7.7 \pm 2.7
Human FFT ^a	5.1	26.5 \pm 1.9	.066 \pm .017	6.0 \pm 0.4	15.5 \pm 4.7
Human HT ^a	21.7	31.5 \pm 3.8	.092 \pm .030	5.13 \pm 0.70	11.7 \pm 3.9

^a From Freeman, Holmes and Vanhatalo. (in preparation), pass band 25-50 Hz, window duration 200 ms, <30% cone residuals.

^b $p < .01$

Table 2.1. The two basic parameters of neocortical EEG, temporal wavelength, W_t , and spatial wavelength, W_x , were evaluated by the Fourier and Hilbert methods. Note the steep gradient by the Hilbert method that was attributed (Table 3) to the use of a short window.

Table 2.2. Means \pm SD of phase cone parameters: FFT/Hilbert

Subject	diameter mm	velocity m/s	duration m/s	interval ms	frame rate Hz
Visual152	14.6 \pm 6.8	1.68 \pm 0.92	88.3 \pm 14.0	77.2 \pm 105	5.1
Hilbert	10.2 \pm 5.0	1.36 \pm .67	4.1 \pm 2.4	69.4 \pm 68.8	3.9
Visual9520	11.4 \pm 5.8	1.25 \pm 0.76	88.3 \pm 14.3	97.5 \pm 125	2.5
Hilbert	8.8 \pm 4.1	1.17 \pm .60	3.88 \pm 2.2	82.1 \pm 91.7	5.0
Auditory531	26.6 \pm 6.6	3.62 \pm 1.20	83.6 \pm 6.1	89.2 \pm 137	3.9
Hilbert	20.4 \pm 8.3	3.24 \pm 1.58	3.35 \pm 2.0	97.2 \pm 117	5.3
Auditory553	14.7 \pm 5.5	1.86 \pm 1.01	86.2 \pm 9.1	78.5 \pm 109	2.9
Hilbert	10.6 \pm 4.97	1.64 \pm 0.83	3.90 \pm 2.2	42.4 \pm 35.9	5.3
Somatic592	16.5 \pm 6.3	2.61 \pm 1.34	88.1 \pm 9.6	127 \pm 153	5.5
Hilbert	12.5 \pm 5.4	2.14 \pm 1.04	3.77 \pm 2.0	49.3 \pm 49.2	5.1
Somatic220	23.9 \pm 7.4	3.28 \pm 1.25	87.1 \pm 11.0	66.4 \pm 92.1	5.4
Hilbert	17.5 \pm 7.6	3.01 \pm 1.42	4.16 \pm 2.4	30.9 \pm 25.6	5.4
Mean FFT	18.0 \pm 6.4	2.38 \pm 1.48	86.9 \pm 9.6	32.3 \pm 30.6	4.2 \pm 1.3
Mean Hilbert	13.3 \pm 4.6	2.09 \pm 0.87	3.9 \pm 0.3	61.9 \pm 25.3	5.0 \pm 0.6
Human FFT ^a	25.2 \pm 6.1	2.67 \pm 0.66	205 \pm 8.6	685 \pm 1280	1.4 \pm 0.8
Human HT ^a	20.6 \pm 14.3	2.55 \pm 1.63	6.2 \pm 3.8	159 \pm 232	3.2 \pm 0.7

^a From Freeman, Holmes, West and Vanhatalo. (submitted), pass band 25-50 Hz, window duration 200 ms, <30% cone residuals.

Table 2.2. The parameters of phase structures in neocortical EEG were derived from spatial and temporal wavelengths by equations (1) to (4). The differences on comparing the results from the two methods were attributed to the differences in window duration (Table 3).

3.3. Measurement of phase gradients with the Hilbert method

ty[The spatial and temporal filter settings and basis functions (cosine, cone) were the same for the Fourier and Hilbert methods, but the windows of measurement differed. The minimal duration for the Fourier method (e.g., 32 ms at 31 Hz) was set by the wavelength of the frequency at which the phase was defined. The minimal duration for the Hilbert method was set by the average wavelength, which determined the interval between break points (Appendix 1.3 in Part 1), minus the range of variation in phase within that wavelength, so that the entire distribution was kept between two successive break points. The ranges of these two windows did not overlap. Referring to Fig. A1.10, B in Part 1, the upper limit on the window length with atan2 was 12 to 20 ms, depending on whether the low pass filter was set at 80 or 50 Hz, in order to stay within the intervals between branch points in the sawtooth given by the mean, $\underline{P}(t)$, without unwrapping.

Measurements of phase by the Fourier and Hilbert methods were expected to correspond within the limitations of the two procedures (Le Van Quyen et al., 2001; Quiroga et al., 2002). In both

methods a phase surface, ϕ_1 or P, was derived centered at each digitizing step and fitted with a cone, Φ , (Appendix 2.2) irrespective branch points and jumps or dips (“phase slip”, Pikovsky, Rosenblum and Kurths, 2001). Identification of stable phase cones was done in accordance with the same criteria as for phase surfaces by the Fourier method, $\phi_{i,j}(t)$, except that there was no % residual from fitting a cosine, and the duration was solely by the number of steps without adding the window duration (Table 2.3). Approximately the same numbers and distributions of cones were found in the same time periods, though without precise correlation in time (Table 2.1, Fig. A2.07, A vs. Fig. 2.03, A) or location (Fig. A2.09, C vs. Fig. A2.02, A). The PSD_T (Fig. A2.07, B and C) and cospectrum (D) were quite similar to those from the Fourier approach (Fig. A2.03), as were the statistics (Tables 1 and 2) and histograms of frequencies (Fig. A2.08, A vs. Fig. 2.03, A), phase gradients and wavelengths (Fig. A2.09 vs. Fig. 2.04). The striking difference (Table 2.2 and Fig. A2.09, B vs. Fig. 2.05) was that the durations of Hilbert-derived cones were far shorter than those of Fourier-derived cones, owing to the restrictions on the two methods. Significant secondary effects were steeper phase gradients and smaller spatial wavelengths by the Hilbert method, leading to lower phase velocities (Fig. A2.09, C vs. Fig. 2.04, A) and half-power diameters (D_x), as described in Section 3.4.

3.4. Dependence of the parameters of phase cones on scales of measurement

The results in Table 2.3 showed that the duration of phase cones and also the intervals between starting times and number of cycles/cone depended on the duration of the window used for measurement. Estimates of the phase gradient were less strongly affected, but all of the parameters derived from that measure were undeniably dependent on the measuring window. The histograms of durations in log-log coordinates (Fig. 2.05, A, C, E) conformed to a power-law distribution, as did the histograms of intervals (not shown), indicating that they were fractal with self-similarity over a varying scale of measurement. Scatter plots of the relation of diameter to duration gave normal distributions of diameter that were self-similar over the 3 Fourier window durations and displayed an increase in diameter with increasing window duration (Fig. 2.05, B, D, F).

An incidental finding listed in Table 2.3 was the increase in number of cycles/cone with increased window duration. Histograms of this parameter conformed to a power-law distribution (Fig. 2.06, A) when derived with a short window, but with a long window there was a distinctive loss of self-similarity with the emergence of a substantial excess of cones having a high number of cycles (E). From the standpoint of the efficacy of cortical dynamics, this excess (also shown in Fig. A1.08 in Part 1) may be the most significant finding of the entire study, because this characteristic might serve to identify a subclass of events that had the persisting coherence of a carrier frequency that would dominate cortical output. Scatter plots of cycles/cone versus frequency (B, D, F) showed that the preponderance of these events were between 3 and 5 cycles/cone at frequencies between 20 and 40 Hz encompassing the high beta and low gamma ranges.

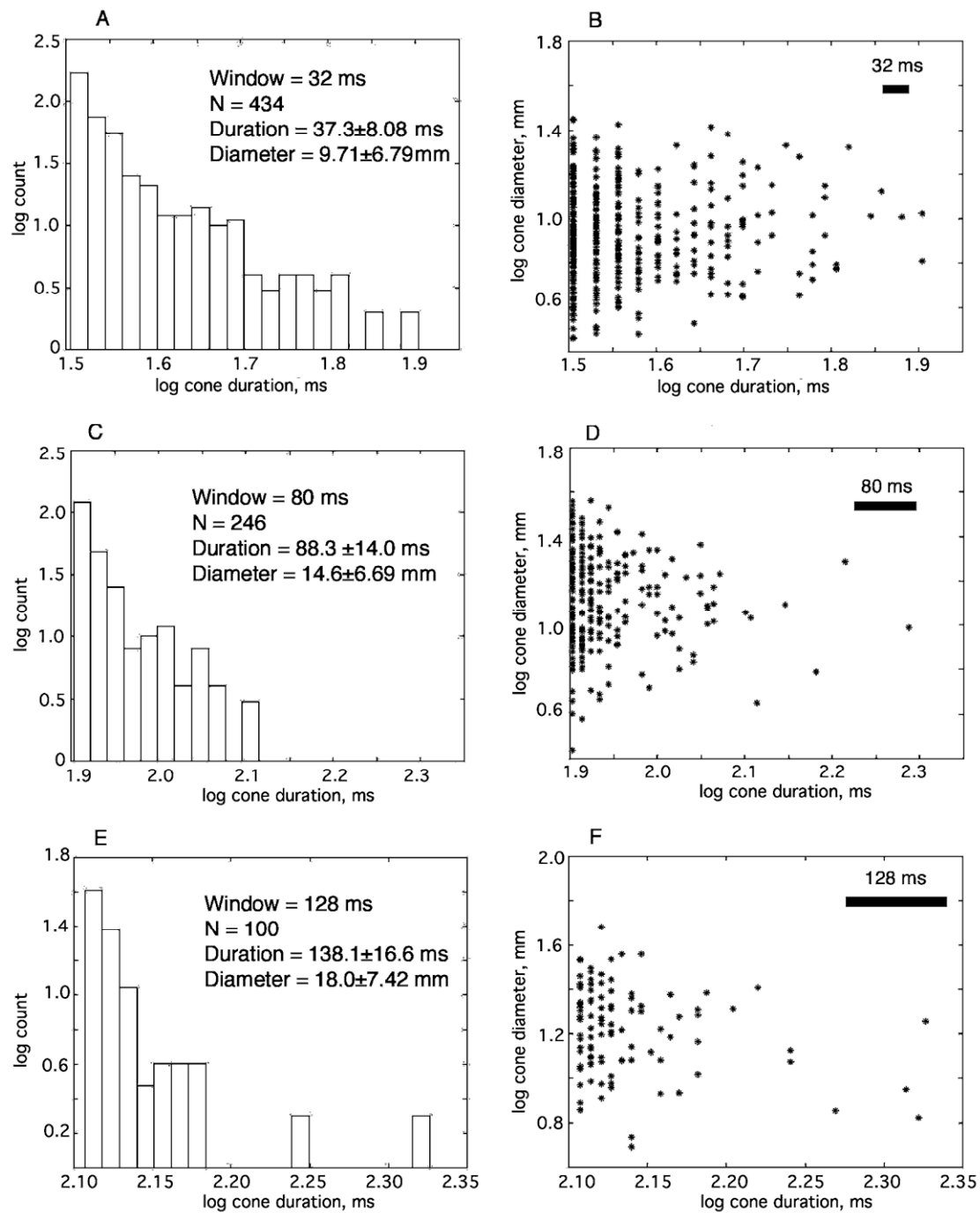


Fig. 2.05. A, B. 32 ms window. C, D. 80 ms window. E, F. 128 ms window. The distributions of cone durations were fractal with maximal numbers at minimal duration and near-linear decrease in log number with increasing log duration. The minimum, mean, SD, and the number of qualifying cones increased with increasing window duration. Cones with log diameter >1.3 (20 mm) were essentially global and included most of the forebrain, as predicted from measurements of global synchrony (Freeman and Rogers, 2003) and global AM patterns (Freeman and Burke, 2003) in gamma EEG.

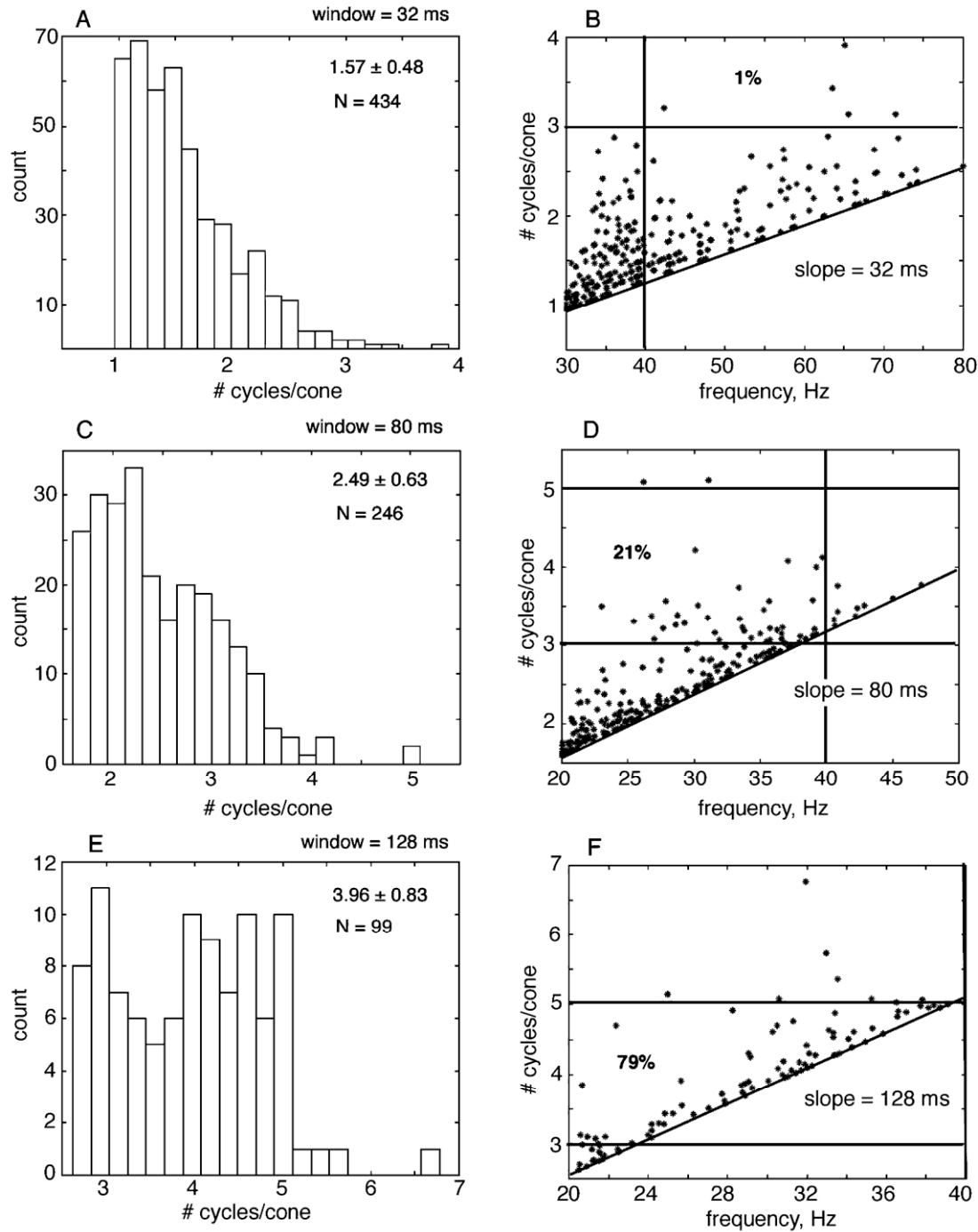


Fig. 2.06. A, C, E. Histograms show the number of cycles in each qualifying cone at the frequency determined by the Fourier method. B, D, F. Scatter plots show the relation between the number of cycles and the frequency. Values are inaccessible below the slope determined by the window duration. The % denotes the proportion of phase cones that have ≥ 3 cycles/cone. The excess number of events above the fractal distribution in frame E indicates a predilection for long-lasting events (see also Fig. 1.08, C and Fig. A1.09, C in Part 1).

Table 2.3. Effects of window duration on results from Hilbert and Fourier transforms

Window	2 ms	32 ms ^a	80 ms	128 ms
Primarily affected:				
Duration, ms	4.1±2.4	37.3±8.1	88.3±14.0	138±16.6
Intervals, ms	69.4±68.8	44.7±51.1	77.2±105	172±287
Cycles/cone, number	.14	1.6	2.5	4.0
Secondarily affected:				
Gradient, γ , rad/mm	0.188±.085	.201±.094	.126±.073	.105±.051
Log W_x , mm/rad	.77±.19	.74±.20	.92±.21	1.01±.19
Velocity, m/s	1.36±0.69	1.61±0.80	1.68±0.92	2.13±1.06
Diameter, mm	10.3±5.0	9.7±4.7	14.6±6.8	18.0±7.4
Distance ^b , mm	2.51±1.20	3.04±1.68	3.19±1.65	3.8±2.5
Unaffected:				
Frequency, Hz	33.7±7.5	42.2±10.9 ^a	28.2±6.1	28.6±5.5
W_r , ms/rad	5.0±1.0	3.99±.87 ^a	5.90±1.20	5.8±1.2
Frame rate, Hz	5.7±.2	5.6±.3	5.7±.2	5.0±.3

- ^a Temporal pass band 30-80 Hz, otherwise 20-80 Hz

- ^b From center of array, half-width 2.8 mm

Table 2.3. Parameter values show the sensitivities of estimates of phase structures to the duration of the window used for measurement.

4. Discussion

4.1. EEG phase data and the concept of self-organized criticality

Phase is easily understood as a difference between the times of zero crossings of two EEG components at the same frequency. The concept is readily generalized to multiple EEG signals by computing the spatial ensemble average and measuring the time difference between each signal and the average as a common reference. It is not difficult to treat aperiodic waveforms as sums of component frequencies, giving a phase distribution for each component and each pair of locations. This empirical approach sufficed for analysis of paleocortical EEG from the olfactory bulb that sustains only one phase cone with each inhalation. This empirical approach suffices for the OB EEG having only one phase cone at a time, but among neocortical EEG signals every phase distribution has multiple cones with different gradients at different frequencies, and they overlap in unpredictable ways. This finding exhausts data-driven analysis. A good hypothesis is needed to organize the data.

One such is provided by the theory of self-organized criticality (“SOC”, Bak, Tang and Wiesenfeld, 1987, Bak, 1996, Jensen, 1998; Watters, 2000) backed by modeling cortical dynamics with nonlinear ordinary differential equations (Freeman, 1975, 2000 and Appendix 2.4). The classic SOC object of study was a sand pile as at the bottom of an hourglass. The steady drip of sand creates a conic pile that increases slope to a critical angle or repose that is held thereafter by repeated avalanches. Likewise a pan of water brought to a boil holds a

constant temperature by forming bubbles of steam. An open system of interacting elements, whether grains of sand, water molecules or neurons, evolves to a stable steady state that is far from equilibrium. That global state is maintained by repeated adjustments: avalanches of sand, bubbles of steam, or phase transitions among groups of neurons. The records of the movements of sand appear chaotic and give temporal and spatial spectra with $1/f^\alpha$ forms. Likewise the EEG gives records that appear chaotic, with temporal and spatial spectra that are $1/f^\alpha$, where the exponent α has been estimated $1 < \alpha < 3$ (Pereda et al., 1998; Freeman et al., 2003). In both systems the appearance of “noise” is illusory. When viewed from the proper perspective, informative structures in the “noise” become clear. The background EEG especially at the scalp reveals a robust, structured dynamics, which manifest the mechanics of self-organization that regulates the multiple brain systems adapting the brain and body to an ever-changing environment.

A way to understand the phase patterns is to see cones as resembling avalanches. Their times and locations of onset are predictable not locally but only in the average. They overlap so that any grain of sand or neuron may participate in multiple cones or avalanches simultaneously. The sizes and durations of cones and avalanches give histograms that are fractal. The smallest and briefest are the most numerous, the distributions in time, space and frequency follow power laws, the patterns are self-similar across multiple scales (Ingber, 1995; Wright and Liley, 1996; Linkenkaer-Hansen, 2001; Hwa and Ferree, 2002), and estimates of the means and SD depend on the size of the measuring tool. These functional similarities indicate that neocortical dynamics is scale-free (Wang and Chen, 2003): the largest events are in the tail of a continuous distribution and share the same mechanism of onset with the smallest and the same brief time of onset despite their large size (Cover Illustration). The spatiotemporal patterns of coordinated analytic phase differences (CAPD) are self-similar over wide scales of time and space, as shown by comparing the rabbit image in Fig. A1.04 in Part 1 with the raster from human scalp data in Fig. A1.12 and those in Freeman, Burke and Holmes (2003).

Though the spatial window was not varied in the present study, data on hand indicate that estimates of the mean diameters of phase cones vary in proportion to the aperture width: 10-12 mm for the olfactory bulb with a 3.5x3.5 mm array (Freeman and Baird, 1987), 18 mm with a 5.6x5.6 mm array in the present study, 25 mm in human temporal cortex with a 10x10 mm subdural array (Freeman et al., in preparation), and several cm on the scalp with an 189 mm linear array with 3 mm spacing (Freeman, Burke and Holmes, 2003). The available evidence indicates that neocortex in mammalian brains of all sizes may conform to a scale-free network (Wang and Chen, 2003) having no characteristic event size; large-scale phase structures (CAPD) seen with scalp EEG arrays and phase cones seen with small intracranial arrays appear to be events of like kind.

4.2. A neural mechanism for self-organized criticality in neocortex

The invariant feature of boiling water is the temperature, and that of the sand pile is the critical angle of repose of the cone. A comparable feature in brains may be the mean level of background activity of neural populations. This feature has been investigated by modeling the dynamics of the olfactory system (Freeman, 1975; Kozma and Freeman, 2001, Appendix 2.4) as mixed populations of excitatory and inhibitory neurons having 3 types of local feedback (mutual

excitation, mutual inhibition, and negative feedback) and long-range excitatory interactions with divergence and distributed delays. The local negative feedback interaction between excitatory and inhibitory neurons supports bulbar oscillations in the gamma range, but only under barrages of input relayed from odorant receptors through the olfactory bulb. When the nasal passages are blocked or the olfactory nerve to the bulb is cut, the gamma oscillations disappear (Becker and Freeman, 1968) in both the bulb and prepyriform cortex, leaving only unstructured background activity: random pulse trains having constant mean rates with SD equal to the means, forming a sheet of steady state activity resembling white noise with dendritic potentials resembling colored noise with $1/f$ spectra. Owing to the lack of structure the basal state is “symmetric”. The hypothesis is proposed that the mean rate of background firing of axons and the mean transcortical d.c. dendritic potential in this state are analogous to the steepness of the critical angle of the sand pile without input, because thresholds and refractory periods provide local homeostatic regulation of neural firing everywhere in normal cortex (Freeman, 1975, 2000; Appendix 2.4). The featureless basal state holds over the whole of the interconnected populations. By this hypothesis input serving as a “control parameter” induces a phase transition that breaks the symmetry (Haken, 1983), leading to the emergence of structure from disorder by virtue of an “order parameter” (Section 4.2 in Part 1). The mechanism of destabilization is provided by the nonlinear gain function that governs the conversion of dendritic wave density to axonal pulse density at the trigger zones in populations of neurons (Freeman, 2000). The inference that the basal state is scale-free implies that the symmetry-breaking can be either by implosion or explosion, meaning lead or lag at the apex of the cone, as observed in the olfactory bulb (Freeman and Baird, 1987) and neocortex (Freeman and Barrie, 2000), and as proposed by Kozma (2003) in terms of the ratio of short to long axonal connections in small-world networks (Watts and Strogatz, 1998). Further mathematical modeling will be needed to determine whether the scale-free dynamics can explain the phase transitions by implosion.

4.3. Conclusion

Under the proposed hypothesis neocortical self-organized dynamics is qualitatively the same in rats, rabbits, cats and humans. The greater size of the human brain’s neocortical neuropil permits the embedding of a larger number of microscopic networks that are specialized for a variety of functions. The repetitive, near-instantaneous reorganization and integration over vast areas of cortex during human cognition are predicted to follow rules similar to those found in animals (Freeman, Gaál and Jornten, 2003; Freeman and Burke, 2003; Freeman and Rogers, 2003), when the subjects are engaged in simpler cognitive tasks. Scalp EEG may prove to be the most valuable means of access to cognitive dynamics in humans, because smoothing by the intervening tissues gives access to the largest patterns. Perhaps by sheer size those patterns may be most likely to constitute Gestalts, which control the brain stem populations that implement behaviors. The problem for understanding the neurodynamics of perception now becomes that of explaining how multiple mesoscopic wave packets that enable “feature binding” of sensory information in mnemonic context (Singer and Gray, 1995) are subsumed into macroscopic Gestalts by global phase transitions.

References

- Ahrens KF, Freeman WJ. Response dynamics of entorhinal cortex in awake, anesthetized and bulbotomized rats. *Brain Res.* 2001, 911: 193-202
- Bak P. *How Nature Works: The Science of Self-organized Criticality.* New York: Copernicus, 1996.
- Bak P, Tang C, Wiesenfeld K. Self-organized criticality: an explanation of 1/f noise. *Phys. Rev. Lett.* 1987, 59: 364-374.
- Barrie JM, Freeman WJ, Lenhart M. Modulation by discriminative training of spatial patterns of gamma EEG amplitude and phase in neocortex of rabbits. *J. Neurophysiol.* 1996, 76: 520-539.
- Becker CJ, Freeman WJ. Prepyriform electrical activity after loss of peripheral or central input or both. *Physiol. Behav.* 1968, 3: 597-599.
- Bullock TH. The neuron doctrine and electrophysiology. *Science* 1969, 129: 997-1002.
- Braitenberg V, Schüz. *A Anatomy of the Cortex: Statistics and Geometry.* Berlin: Springer-Verlag, 1991.
- Elul R. The genesis of the EEG. *Intern. Rev. Neurobiol.* 1972, 15:227-272,
- Freeman WJ. *Mass Action in the Nervous System.* Academic Press, New York, 1975.
Reprinted 2004: <http://sulcus.berkeley.edu/MANSWWW/MANSWWW.html>
- Freeman WJ. Strange attractors that govern mammalian brain dynamics shown by trajectories of electroencephalographic (EEG) potential. *IEEE Trans. Circuits Systems* 1988, 35: 781-783.
- Freeman WJ On the problem of anomalous dispersion in chaoto-chaotic phase transitions of neural masses, and its significance for the management of perceptual information in brains. Ch. in: Haken H, Stadler M (eds.) *Synergetics of Cognition.* Berlin, Springer-Verlag, 1990, Vol. 45: 126-143.
- Freeman WJ Valium, histamine and neural networks. *Biol. Psychiat.* 1993, 34: 1-2.
- Freeman WJ. *Neurodynamics. An Exploration of Mesoscopic Brain Dynamics.* London UK: Springer-Verlag, 2000.
- Freeman WJ. *How Brains Make Up Their Minds.* New York: Columbia U.P., 2001.
- Freeman WJ. A neurobiological theory of meaning in perception. Part 1. Information and meaning in nonconvergent and nonlocal brain dynamics. *Int. J. Bifurc. Chaos* 2003a, 13: 2493-2511.
- Freeman WJ. A neurobiological theory of meaning in perception. Part 2. Spatial patterns of phase in gamma EEG from primary sensory cortices reveal the properties of mesoscopic wave packets. *Int. J. Bifurc. Chaos* 2003b, 13: 2513-2535.
- Freeman WJ. Origin, structure and role of background EEG activity. Part 1. Analytic amplitude. *Clin. Neurophysiol.* 2004, In press.
- Freeman WJ, Baird, B. Relation of olfactory EEG to behavior: Spatial analysis: *Behav. Neurosci.* 1987, 101: 393-408.
- Freeman WJ, Barrie JM. Analysis of spatial patterns of phase in neocortical gamma EEGs in rabbit. *J. Neurophysiol.* 2000, 84: 1266-1278.
- Freeman WJ, Burke BC. A neurobiological theory of meaning in perception. Part 4. Multicortical patterns of amplitude modulation in gamma EEG *Int. J. Bifurc. Chaos* 2003, 13: 2857-2866.
- Freeman WJ, Burke BC, Holmes MD. Aperiodic phase re-setting in scalp EEG of beta-gamma oscillations by phase transitions at alpha-theta rates. *Hum Brain Mapp* 2003, 19: 248-272.

- Freeman WJ, Burke BC, Holmes MD, Vanhatalo S. Spatial spectra of scalp EEG and EMG from awake humans. *Clin. Neurophysiol.* 2003, 16: 1055-1060.
- Freeman WJ, Gaál G, Jornten, R. A neurobiological theory of meaning in perception. Part 3. Multiple cortical areas synchronize without loss of local autonomy. *Int. J. Bifurc. Chaos* 2003, 13: 2845-2856.
- Freeman WJ, Grajski KA. Relation of olfactory EEG to behavior: Factor analysis. *Behav. Neurosci.* 1987, 101: 766-777.
- Freeman WJ, Holmes MD, West GA, Vanhatalo S. Spatiotemporal infrastructure of phase in human intracranial EEG. In preparation.
- Freeman WJ, Rogers LJ. Fine temporal resolution of analytic phase reveals episodic synchronization by state transitions in gamma EEGs. *J. Neurophysiol.* 2002, 87: 937-945.
- Freeman WJ, Rogers L.J. A neurobiological theory of meaning in perception. Part 5. Multicortical patterns of phase modulation in gamma EEG. *Int. J. Bifurc. Chaos* 2003, 13: 2867-2887.
- Freeman WJ, Viana Di Prisco G. Relation of olfactory EEG to behavior: Time series analysis. *Behav. Neurosci.* 1986, 100: 753-763.
- Gray CM, Skinner JE. Centrifugal regulation of neuronal activity in the olfactory bulb of the waking rabbit as revealed by reversible cryogenic blockade. *Exp. Brain Res.* 1988, 69:378-386.
- Haken H. *Synergetics. An Introduction.* Berlin: Springer-Verlag, 1983.
- Hwa RC and Ferree T. Scaling properties of fluctuations in the human electroencephalogram. *Physical Rev.* 2002, E 66: 021901.
- Ingber L. Statistical mechanics of multiple scales of neocortical interactions. pp. 628-681 in: Nunez, P.L. (ed.) *Neocortical Dynamics and Human EEG Rhythms.* Oxford UP, New York, 1995.
- Jensen HJ. *Self-Organized Criticality: Emergent Complex Behavior in Physical and Biological Systems.* New York: Cambridge UP, 1998.
- Kozma R. Personal communication, 2003.
- Kozma R, Freeman WJ. Chaotic resonance: Methods and applications for robust classification of noisy and variable patterns. *Int. J. Bifurc. Chaos* 2001, 10: 2307-2322.
- Kozma R, Freeman WJ, Erdí P. The KIV model – nonlinear spatio-temporal dynamics of the primordial vertebrate forebrain. *Neurocomputing* 2003, 52: 819-826.
- Le Van Quyen M, Foucher J, Lachaux J-P, Rodriguez E, Lutz A, Martinerie J, Varela F. Comparison of Hilbert transform and wavelet methods for the analysis of neuronal synchrony. *J. Neurosci. Meth.* 2001, 111: 83-98.
- Linkenkaer-Hansen K, Nikouline VM, Palva, JM, Iimoniemi RJ. Long-range temporal correlations and scaling behavior in human brain oscillations. *J Neurosci* 2001, 15: 1370-1377.
- Mandelbrot BB. *The Fractal Geometry of Nature.* New York: W H Freeman, 1983.
- Miller LM, Schreiner CE. Stimulus-based state control in the thalamocortical system. *J Neurosci.* 2000: 20:7011-7016.
- Ohl FW, Scheich H, Freeman WJ. Change in pattern of ongoing cortical activity with auditory category learning. *Nature* 2001, 412: 733-736.
- Pereda E, Gamundi A, Rial R, Gonzalez J. Non-linear behavior of human EEG – fractal exponent versus correlation dimension in awake and sleep stages. *Neurosci. Lett.* 1998, 250: 91-94.

- Pikovsky A, Rosenblum M, Kurths J. Synchronization — A Universal Concept in Non-linear Sciences. Cambridge UK: Cambridge University Press, 2001.
- Principe JC, Tavares, VG, Harris JG, Freeman WJ. Design and implementation of a biologically realistic olfactory cortex in analog VLSI. Proc. IEEE 2001; 89: 1030-1051.
- Quiroga RQ, Kraskov A, Kreuz T, Grassberger P. Performance of different synchronization measures in real data: A case study on electroencephalographic signals. Physical Rev E 2002, 6504:U645-U658 - art. no. 041903.
- Singer W, Gray CM. Visual feature integration and the temporal correlation hypothesis. Ann Rev Neurosci. 1995, 18: 555-586.
- Steriade M. Synchronized activities in coupled oscillators in the cerebral cortex and thalamus at different levels of vigilance. Cereb. Cortex 1997, 7: 583-604.
- Viana Di Prisco G, Freeman WJ (1985) Odor-related bulbar EEG spatial pattern analysis during appetitive conditioning in rabbits. Behav. Neurosci. 1985, 99: 962-978.
- von der Malsburg C (1983) How are nervous structures organized? In: Basar E, Flohr H, Haken H, Mandell AJ (eds.) Synergetics of the Brain, Berlin: Springer-Verlag, pp. 238-249.
- Wright JJ, Liley DTJ. Dynamics of the brain at global and microscopic scales: Neural networks and the EEG. Behav. Brain Sci. 1996, 19: 285-295.
- Wang XF, Chen GR. Complex networks: small-world, scale-free and beyond. IEEE Circuits Syst. 2003, 31: 6-20.
- Watters PA. Time-invariant long-range correlations in electroencephalogram dynamics, Int. J. Systems Sci. 2000, 31: 819-825.
- Watts DJ, Strogatz SH. Collective dynamics of “small-world” networks. Nature 1998, 393: 440-442.

Appendix 2.1. Temporal basis functions for measuring frequency and phase

The 64 EEG signals were filtered in each trial first spatially (Appendix 1.2) and then temporally (Appendix 1.1) and segmented with an overlapping window 32, 40 or 64 bins in length, stepped at 2 ms intervals for a total of 2000 steps (4 s). The spatial ensemble average was calculated of the 64 EEG in each window (Fig. A2.01). Its FFT gave the temporal PSD_T from which the frequency was found at peak power in the window. The ensemble average was fitted using nonlinear regression with the cosine having that frequency as an initial guess. After regression the fitted cosine at the new frequency, f_1 , was subtracted from the EEG. The FFT was taken of the difference to find a second frequency, f_2 , at peak power by regression. These 2 frequencies

were fixed, and the 2 phase values served as initial guesses for nonlinear regression to fit the sum of the two cosines from equation (Fig. A2.01) to each of the 64 EEG segments by minimizing the sum of least square residuals while allowing the phase, $\phi_j(t)$, and amplitude, $V_j(t)$ to vary:

$$V_j(T) = \sum V_{i,j}(t) \cos [2\pi f_i T + \phi_{i,j}(t)] + R(T), \quad i = 1,2; \quad T = 1, w; \quad j = 1,64 . \quad (\text{A2.1})$$

where T denoted time within a window of length w starting at time t , $V_j(T)$ was the fitted curve, and $R(T)$ denoted the residuals. The larger component served to estimate the frequency, f_1 , of the carrier oscillation in the window, and the lesser component served to filter non-white noise (clutter) from the signal (Freeman, 1975) and improve the signal-to-noise ratio. Equation (A2.1) with fixed frequencies gave the desired 8x8 phase surface at each time step, $\phi_{1,j}(t)$, $j = 1,64$, $t = 1$, for the dominant component at the fixed frequency, using the phase of the ensemble average as the reference. The criterion of goodness of fit was minimization of the least squares residuals expressed as % of the total variance. The % residuals fluctuated erratically with time (Fig. 2.02, D in text).

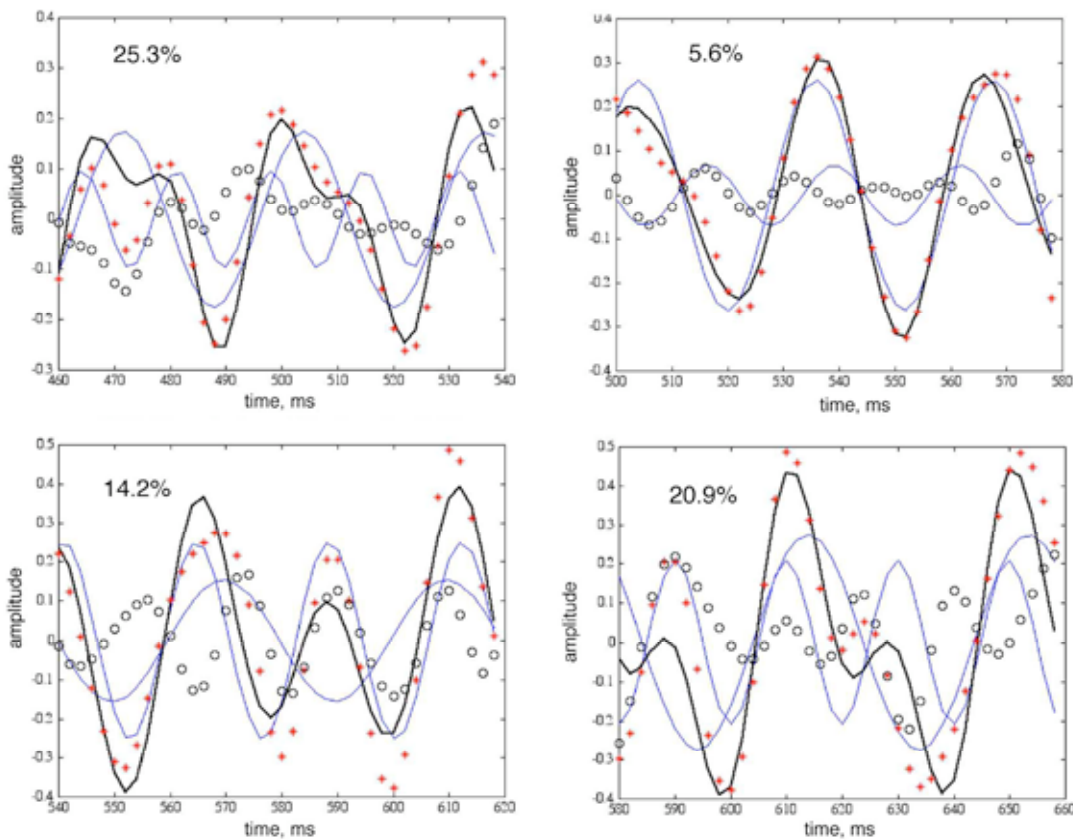


Fig. A2.01. Examples are shown in 80 ms windows of fitting the sum [dark curve] of 2 cosines [light curves] to the digitized, filtered EEG [solid dots] with the residuals [open dots] from a single channel. The ratio off the sum of squares of the residuals to the sum of squares of the data times 100 gave the % residuals. The threshold for an acceptable fit was 20%.

Appendix 2.2. Spatial basis function for measuring phase gradients

The algorithm for preparatory spatial filtering was given in Appendix 1.2 (Part 1). An important methodological difference here was that in previous work the spatial filter was applied to the 8x8 phase matrix, whereas in the present study the spatial filter was applied to the EEGs before determination of the frequencies and phases. A comparison was undertaken to evaluate the degree to which the spatial filter applied to the phase surfaces (Table A2.1, A, Methods 1-3) had biased earlier estimates of the gradients of the fitted cones by making them appear steeper than was the case, and altered the locations of their apices by making them appear closer to the center of the array than was the case (Freeman and Barrie, 2000). The standard adopted for reference was Method 4 (B in Table A2.1) using the FFT. Method 2 using nonlinear wavelets (Freeman, 2003b) gave parameters that most closely approximated those of Method 4, followed by Method 6 using the spatial SD_j of $\phi_{1,j}(t)$ and $P_j(t)$ for the criteria to identify qualifying phase cones (Appendix A1.3 and Fig. A1.10). The Hilbert Method 5 also overestimated the phase gradients, γ_k , owing to the short duration of the window (Table 2.3) that distorted estimates of phase gradient, velocity, diameter and distance.

The spatial pattern of phase was measured by fitting a cone, $\Phi(t)$, in 2-D to the 8x8 phase surface, either $\phi_{1,j}(t)$ from the Fourier method or $P_j(t)$ from the atan2 function (equation (A1.5) in Appendix 1.3), at each window step, Δt (2 ms), by using nonlinear regression to fit $\Phi(t)$ in equation (A2.2) to the surface with termination of iteration by minimization of least squares residuals:

$$\Phi(t) = \Phi_o(t) + \gamma(t) ([x_j - x_o]^2 + [y_j - y_o]^2)^{-5}, \quad j = 1, 64, \quad (\text{A2.2})$$

where $\Phi_o(t)$ was the offset of the vertical offset apex from the plane of fit, x_j , y_j gave the distance of the apex in mm from the center of the electrode array at x_o , y_o , and $\gamma(t)$ was the gradient of the cone in rad/mm in the t-th step of the window. Two passes were made with each phase surface, one with the location of the phase maximum as the starting guess, the other with the phase minimum for initiation. The result was selected that had the least number of iterations to completion. On average convergence to solutions was achieved in >90-95% of windows with cones. Attempts to fit two cones simultaneously to the same phase surface did not converge. The % residuals was given by:

$$\% \text{ residual} = 1/j \sum^j [\Phi_j(t) - \phi_{1,j}(t)]^2 / \sum^j [\phi_{1,j}(t)]^2, \quad (\text{A2.3})$$

or $P_j(t)$ in place of $\phi_{1,j}(t)$. The value for $\gamma(t)$ was averaged:

$$\gamma_k = \sum^n \gamma(t_n), \quad (\text{A2.4})$$

where n was the number of time steps across which a stable phase cone had been defined. The frequencies, f_i , were similarly averaged to get f_k for the k-th cone, Φ_k . Comparing the residuals from the filtered (Fig. A2.04, A) and unfiltered (Fig. A2.04, B) EEG data showed that filtering substantially reduced the % residuals without significantly altering their temporal structure.

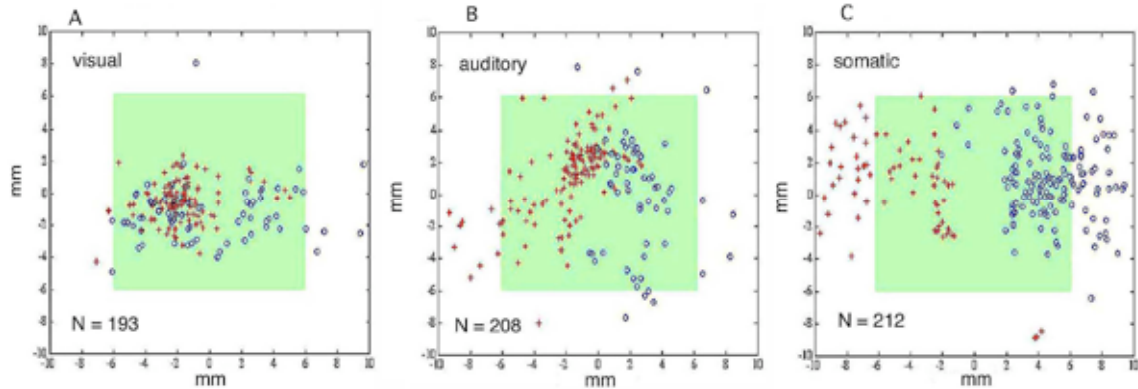


Fig. A2.02. The locations of apices of qualifying cones are shown as + for phase lead and o for phase lag from three cortices. The inset rectangle shows the 5.6x5.6 mm array. The segregation of the apices by sign in data from the somatic cortices is unexplained.

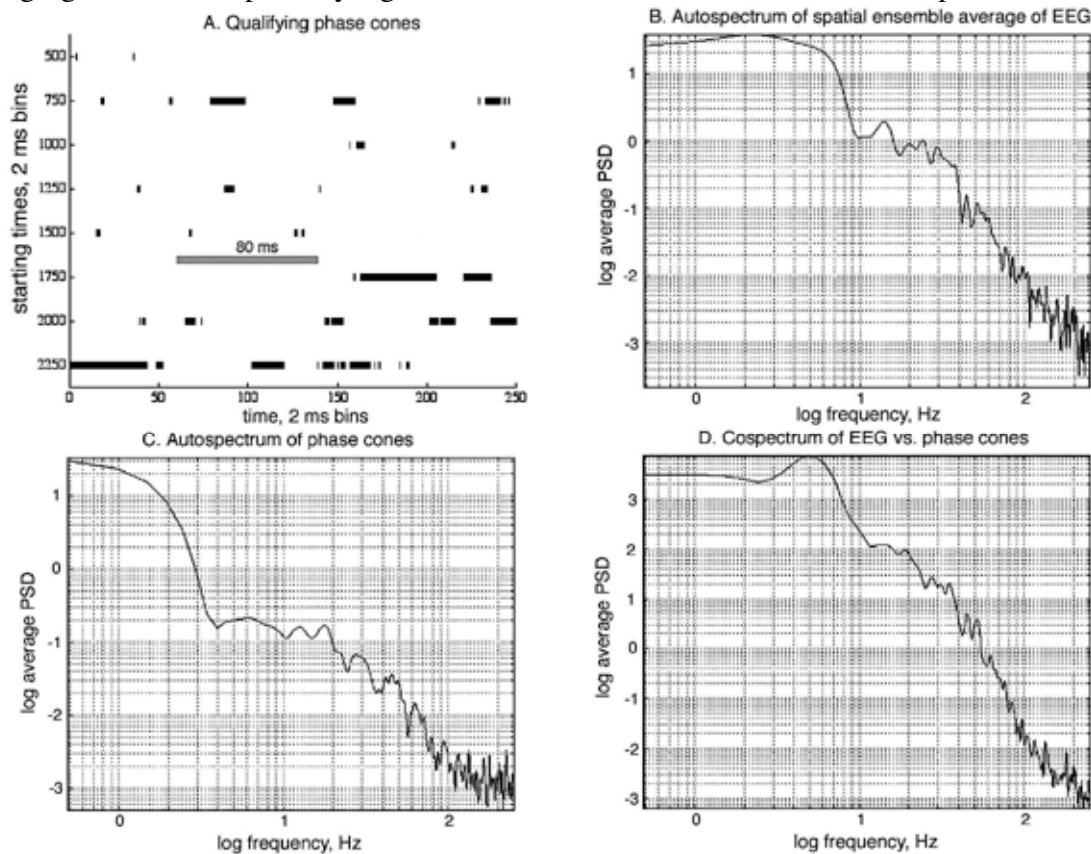


Fig. A2.03. A. The example shows the time series of qualifying cones (less the 80 ms window length) in 2000 steps (4 s). Each bar shows only the number of steps across which it was tracked. The actual duration was that number plus the 40-step (80 ms) window (see inset bar). That bar was omitted because the overlap of cones would have obscured the display. B. The PSD_t of the EEG was taken from the autocorrelation over 5 trials totaling 20 s. C. The PSD_t was taken of the autocorrelation of the phase cones (less the 80 ms window) treated as a step function (black = 1, white = 0). D. The cospectrum from the cross-correlation of EEGs and phase cones revealed a peak in the theta range.

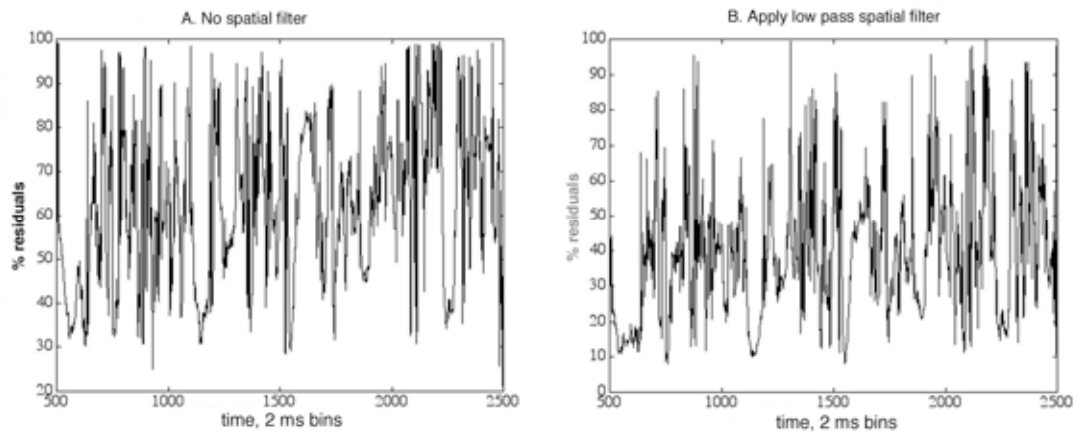


Fig. A2.04. **A.** The % residuals are shown for an 80 ms moving window stepped at 2 ms in a representative time segment lasting 2000 bins (4 s) with no spatial filter. **B.** The % residuals were re-calculated after spatial filtering at the low pass setting shown in Fig. A1.02, B (Part 1). The values were reduced with little effect on the temporal structure of the sequence of % residuals.

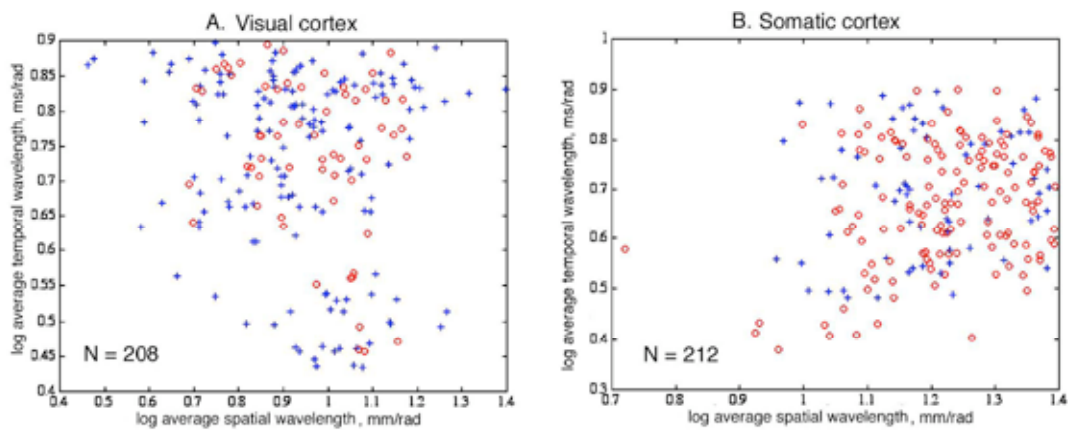


Fig. A2.05. The log values of temporal and spatial wavelength, W_t and W_x , were uncorrelated, irrespective of the sign of the gradient (+ = lead, o = lag).

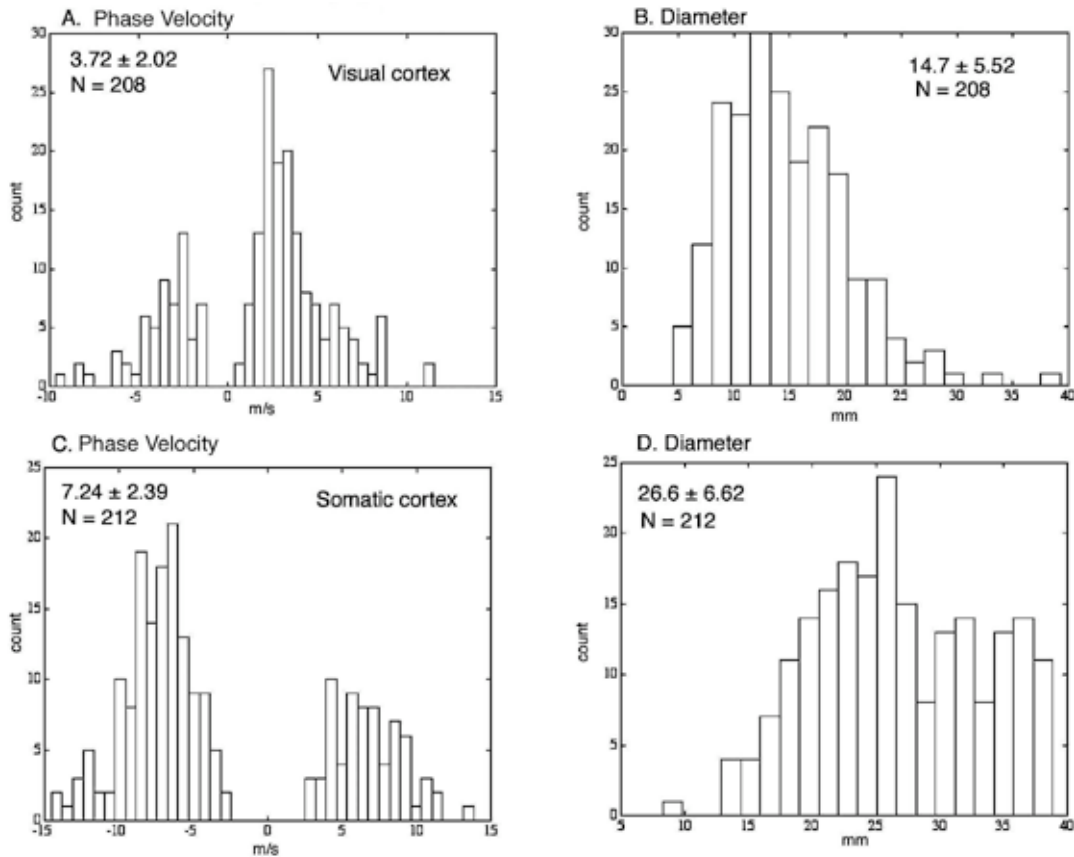


Fig. A2.06. A, C. Phase velocity, β , was calculated from the gradient and frequency with equation (4) giving bimodal distributions.
B, D. Cone diameter was estimated from absolute value of the gradient by equation (3). The distributions were skewed in relation to the asymmetry of β . Most likely the distributions are fractal like those for duration but truncated at the lower end by a combination of spatial filtering and volume conduction.

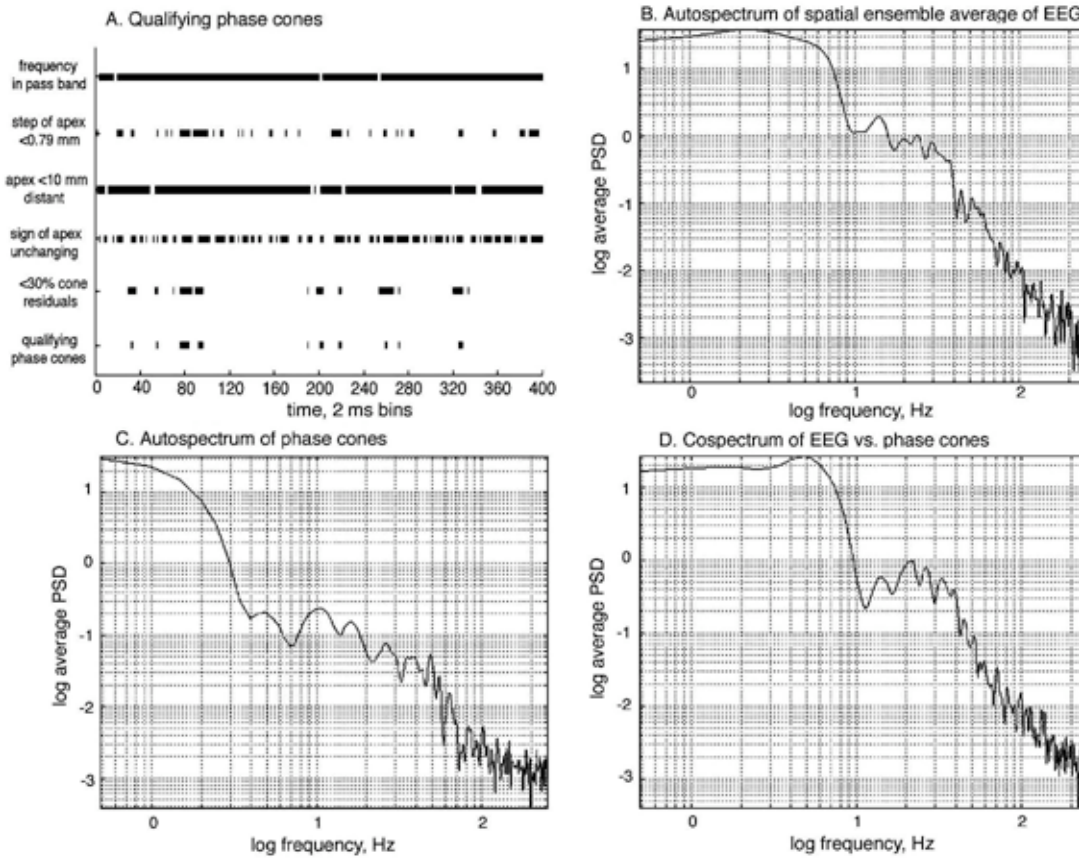


Fig. A2.07. **A.** The same criteria used to qualify phase cones derived from FFT (Fig. A2.03) were applied to the analytic phase surfaces.
B. The PSD_i of the EEG was calculated from the autocorrelation of the spatial ensemble average of the unfiltered EEG across five 4 s trials.
C. The PSD_i of the phase cones was calculated from the autocorrelation of the qualifying cones exemplified in frame A.
D. The cospectrum was calculated from the cross-correlation of the EEG and qualifying phase cones as in Fig. A2.03, D.

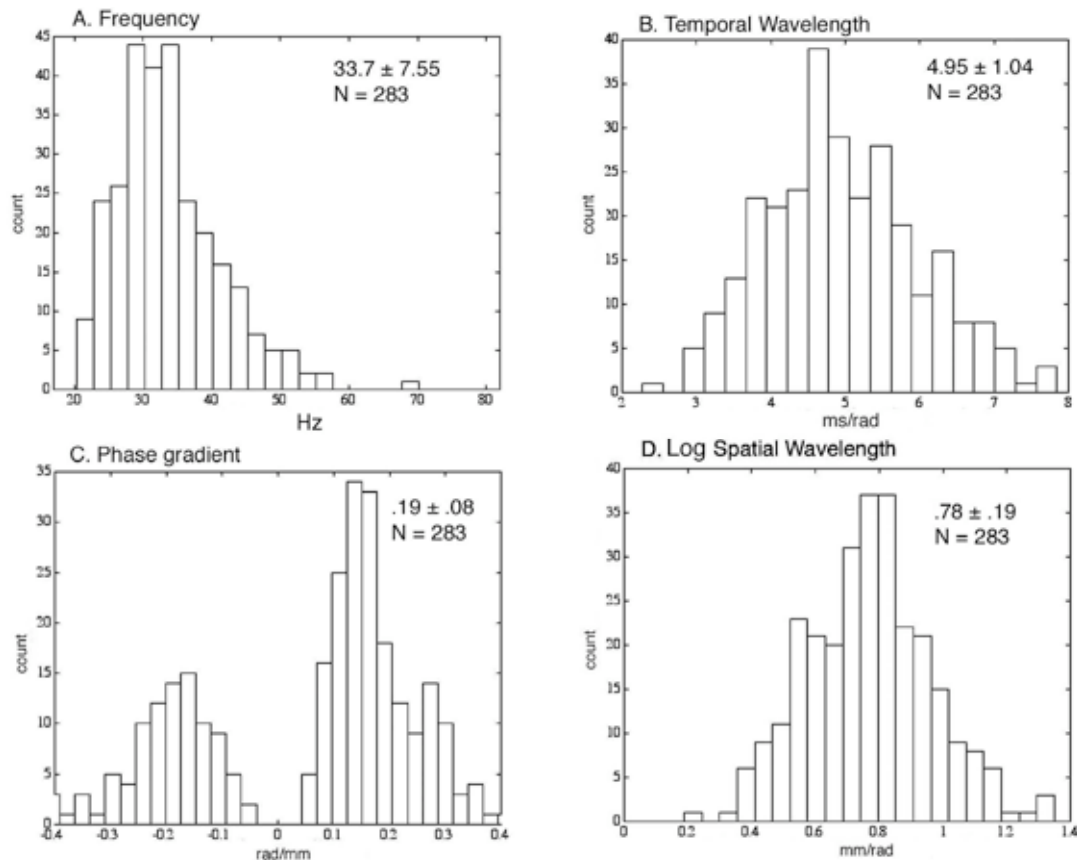


Fig. A2.08. A. Frequency was calculated from the average of the analytic phase differences in the visual cortical EEG in the period of each stable phase cone after unwrapping (see Fig. 2.03, A and Table 1).

B. Temporal wavelength, W_t , was calculated as in Fig. 2.03, B.

C. Phase gradients from cones, Φ , fitted to analytic phase surfaces, P , without unwrapping (Appendix 1.3) were steeper than ϕ_1 from the Fourier method (Fig. 2.04, A and Table 2.2).

D. Spatial wavelengths, W_x , appeared to be shorter (Fig. 2.04, B) owing to the shorter window of measurement.

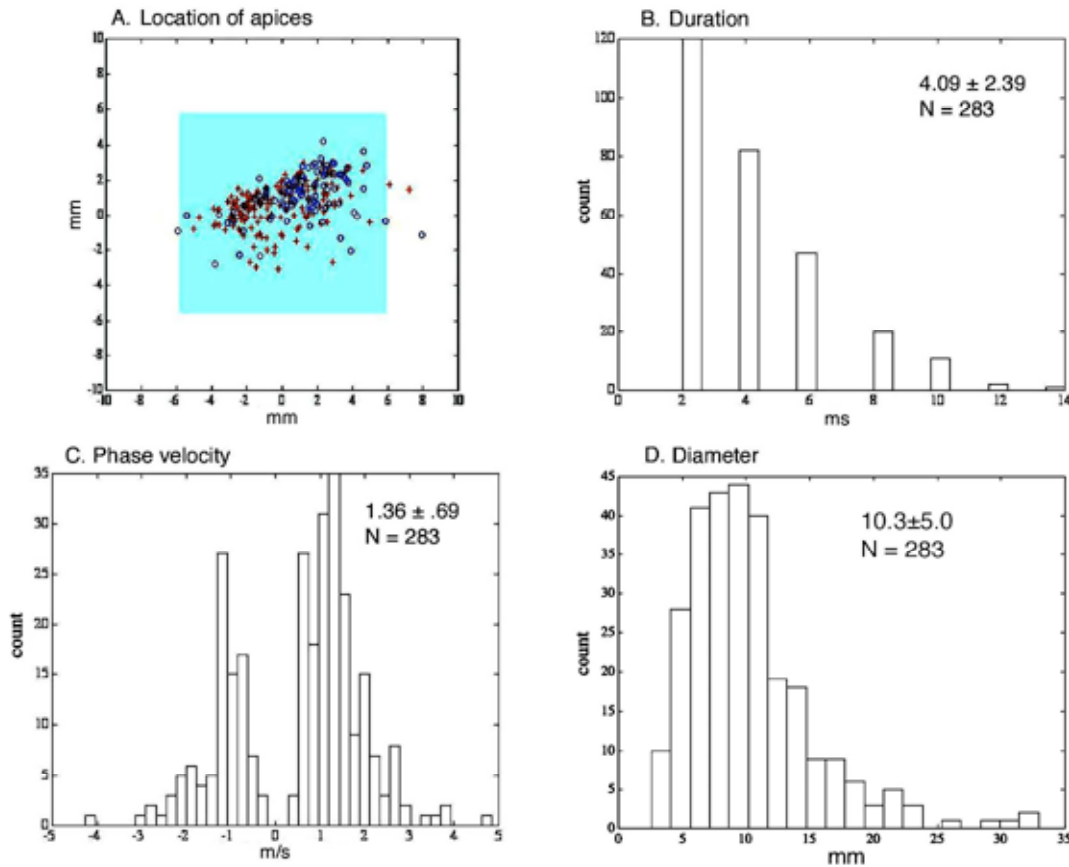


Fig. A2.09. **A.** Locations of apices by the Hilbert method closely resembled those from the Fourier method in location and sign (Fig. 3, A).
B. Estimates of duration were severely limited by the branch points (Appendix 1.3) in deriving Φ (Table 2.2).
C. Analytic phase velocities were slower (see Fig. 2.06, A and Table 3).
D. Analytic phase cone diameter was smaller than the phase cone diameter from the Fourier method (Fig A2.06, B).

Appendix 2.3. Controls by randomization of the EEG data.

The cosine and the cone were simple basis functions that could fit any structure in noise. The spatial and temporal filters needed to measure phase patterns (Fig. XI, A on p. 267 in Freeman, 2000) imposed artificial structure in the EEG data by enhancing oscillation at the center frequency of the temporal pass band, and by enhancing a conic pattern with its apex of either sign at the center of the array (Table A2.1, A). The $1/f^\alpha$ distributions of frequencies, f_1 , in log-log coordinates and the scatter of the apices often outside the array (Fig. A2.02 and Fig. A2.09) showed that the filters did not significantly bias the parameter values of the stable cones with low residuals. The question arose, whether phase cones existed in fractal distributions, such that many of the cones with residuals $>30\%$ were intrinsic to the data. An answer was sought by randomizing the EEG data before filtering and curve fitting. The phase in the PSD_T was

randomized to give surrogate data with reduced temporal structure. The channel order was randomized to reduce spatial structure. Shuffling (Freeman and Rogers, 2002) randomized in both the temporal and spatial domains:

$$v_k(t) = [v_{1,j}(r, r+1, \dots, 64), v_{1,j}(1, 2, \dots, r-1)], \quad (\text{A2.5})$$

where $\phi_{1,j}(t)$ was the original phase time series of 64 points for one channel, and r was a point chosen from a uniformly distributed random variable with values from 1 to 64.

Comparing histograms of the % residuals (Fig. A2.10) showed the effects of randomization on the results first on fitting cosines (A) and then on fitting cones (B). The test data were from 5 trials in one session and animal, each with 2000 digitizing steps (4 s) totaling 20 sec of recording. The asterisk in each frame shows the threshold previously adopted (Freeman and Barrie, 2000) for qualifying segments (20% in the time domain and 30% in the spatial domain). The surrogate data showed reduction in the total number of convergences of regression in curve fitting (C) and modest increases in residuals when convergence was achieved in fitting cones (D). Shuffling had little effect on fitting cosines (E), but it completely blocked convergence on fitting cones. Channel randomization had no effect on fitting cosines, but it substantially increased the residuals on fitting cones (F).

On the basis of finding time-invariant, long-range correlations, Watters (2000) concluded that the distributions of key properties of the EEG are fractal, which is in accord with a state of self-organized criticality. The present results have shown that the phase surface in every time period and area of cortex contained a fractal distribution of co-existing phase cones that formed by mesoscopic phase transitions. Most of these phase cones were rejected by the criteria of the % residuals, which were designed to exclude spurious results from fitting noise. However, the mean estimates of the temporal and spatial wavelengths, W_t and W_x , of the full distributions did not differ from those of the restricted subset (Table A2.2), nor did the derived estimates of phase velocity and half-power diameter (Fig. A2.11, A).

The effect of phase randomization in the surrogate data was to increase the phase gradients and decrease both the velocities and the diameters (Fig. A2.11, B), because the randomization in the surrogate EEGs introduced high spatial frequency noise into the phase surfaces. The effect of channel randomization was the reverse: a substantial increase in phase velocities and diameters (Fig. A2.11, C). The mean diameter approached the length of the rabbit brain (4 cm). These changes were consistent with flattening of the phase matrices by channel randomization, so that the phase gradients were very low and thereby gave inflated estimates of spatial wavelength, phase velocity and cone diameter. The mean distance of apices from the center of the array was decreased slightly with surrogate data and channel randomization. This could not be tested with shuffling, which effectively destroyed the conic phase structure (see also Fig. 16 in Freeman, Burke and Holmes, 2003). The conclusion was that a majority of phase cones in the EEG data with % residuals >30% belonged to the self-organized fractal distribution, and that a minority resulted from fitting the cone to noise.

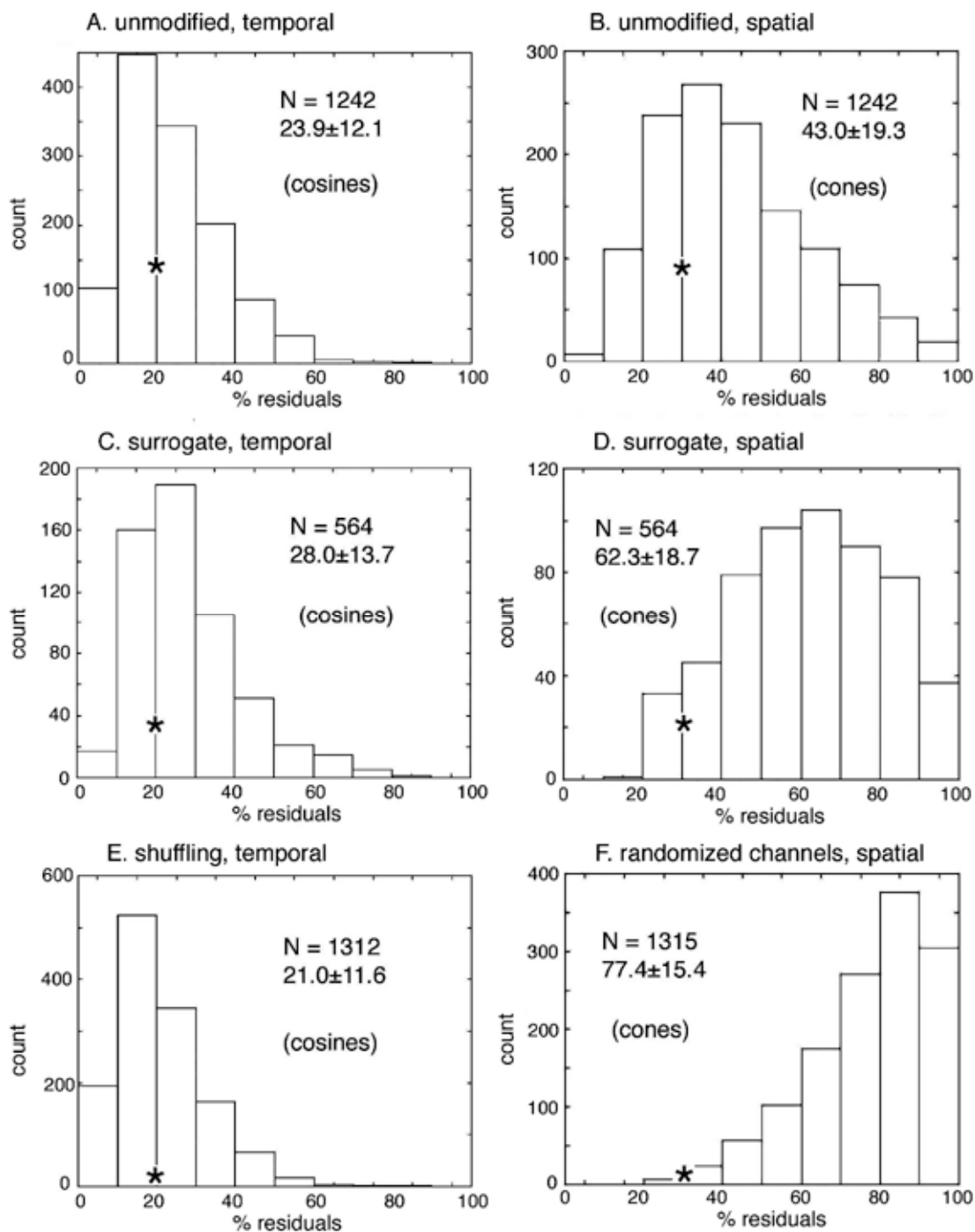


Fig. A2.10. The distributions are shown of the % residuals from fitting cosines (A) and cones (B) to the 80 ms windows in 4 s of EEGs from 5 trials totaling 20 s and selecting those cones that qualified under the first 4 criteria shown in Fig. 2.02, A.

C, D. The procedure was repeated on surrogate EEG data.

E. Shuffling had little effect on cosine residuals, but it abolished cone fits.

F. Channel randomization had no effect on cone fits. Very few cones qualified after shuffling. The asterixes indicate the criteria adopted for qualifying results from regression (Fig. 2.02, A).

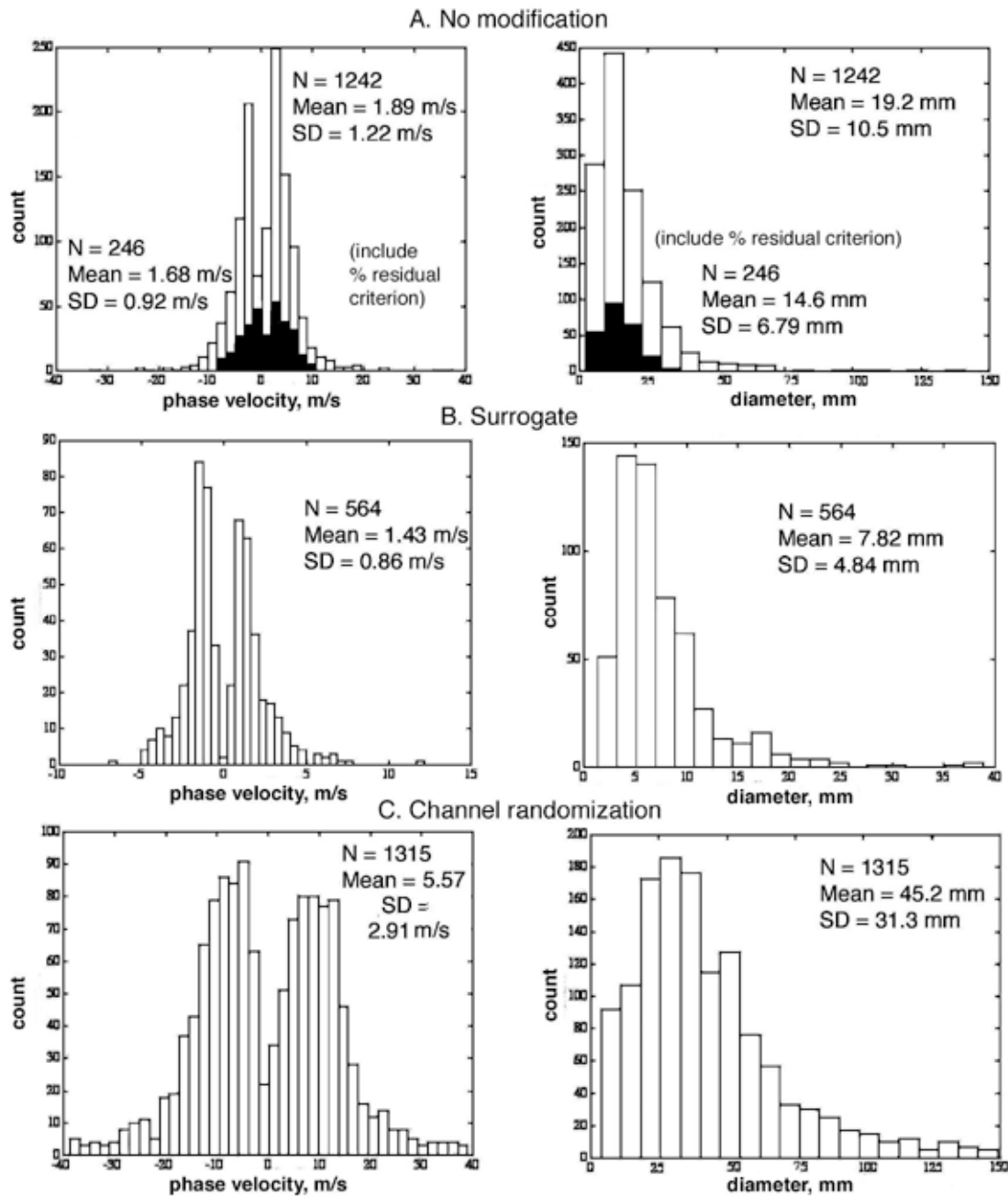


Fig. A2.11. A. The distributions are shown of the values for phase velocity (left) and diameter (right) of qualifying cones before (light bars) and after (dark bars) exclusion by the % residual criteria. Exclusion reduced the means and SD.

B. The surrogate data showed decrease in values for phase velocity and diameters by an increase in the high spatial frequencies of the phase surfaces.

C. Channel randomization increased estimates of phase velocity and diameter by flattening the phase surfaces.

Appendix 2.4. Mathematical basis to model neocortex at self-organized criticality (SOC)

Brains maintain immense numbers of largely autonomous neurons whose main function is keeping themselves alive and healthy for the life span of their host. They are unique among cells in having long filaments by which they interact with others at near and far distances. Modeling of the dynamics of mass actions among populations of neurons (Freeman, 1975, 2004) has been done with a hierarchy of K-sets (for Katchalsky).

A KO set represents a non-interacting collection of neurons that can be described as an average neuron with a state-dependent, linear, 2nd order ordinary differential equation (ODE) for dendritic integration and a sigmoid static nonlinearity for axon transmission. The KO set is governed by a point attractor with zero output and stays at equilibrium except when perturbed.

A KI_c set represents a collection of excitatory neurons that has sufficient functional connection density to maintain a state of background activity by mutual excitation (positive feedback), by which it normally operates far from thermodynamic equilibrium. Its dynamics are described with 2 two coupled KO sets and piece-wise linearization of the ordinary differential equations at the operating point. The equations have a Lyapunov exponent with zero real and imaginary parts representing a point attractor with non-zero output. The stability of the KI_c set under impulse perturbation is demonstrated using the periglomerular cells in the olfactory bulb (summarized in Fig. 2, p. 198 in Freeman, 2000). Its critical contribution is the sustained level of excitatory output that it sends into the bulb, from which it is relayed to the prepyriform and other parts of the forebrain. The set point (level of sustained excitatory output) appears to be governed by histaminergic nuclei in the hypothalamus in conjunction with arousal. Neural interaction by stable mutual excitation is a key to understanding SOC in brains.

A KII set represents a collection of excitatory and inhibitory cells described by KI_c and KI_i sets, having three types of feedback: positive excitatory, positive inhibitory, and negative. Under sustained excitation from a KI_c set but without the equivalent of sensory input, the KII set is governed by the zero Lyapunov exponent of the KI_c set (summarized in Fig. 5 on p. 110 in Freeman, 2000). With simulated sensory input comprising a control parameter the KII set undergoes a phase transition to oscillation at a narrow band frequency in the gamma range (Gray and Skinner, 1988; Ahrens and Freeman, 2001). This state is governed by a limit cycle attractor with a Lyapunov exponent with zero real and non-zero imaginary parts (summarized in Fig. 7.17 on p. 442 in Freeman, 1975; Principe et al., 2001). KII has both point and limit cycle attractors.

A KIII set is formed by the interaction of 3 KII sets through long axonal pathways with distributed delays. It simulates the dynamics of the bulb, prepyriform and anterior nucleus that together generate aperiodic, chaotic oscillations with $1/f^\alpha$ spectra (Kozma and Freeman, 2001). The KIII set is governed by a chaotic attractor having at least one positive Lyapunov exponent (Freeman, 1988). It is stabilized by the KI_c mechanism but gives no evidence of SOC. A KIV set is formed by the interaction of 3 KIII sets. It is used to model the interactions of the primordial vertebrate forebrain in the genesis of simple forms of intentional behavior (Kozma, Freeman and Erdí, 2003). It, too, is stable but does not display SOC.

A KV set is proposed to model the unique properties of neocortex, which maintains multiple unstable periodic orbits that appear as overlapping phase cones. It is postulated that the robust background activity of the neocortex manifests the continuous engagement of the organism with its environment. Sensory-driven thalamic input to cortex is described as a control parameter (Steriade, 1997; Miller and Schreiner, 2000) that induces the oscillations observed in the EEG and in the classic spectral peaks. In the absence of such input the endogenous truly “spontaneous” activity would be that maintained at self-organized criticality by mutual excitation that is governed by a global point attractor. This much has been shown experimentally (Freeman, 2000; Kozma and Freeman, 2001; Principe et al., 2001). Proof using nonlinear differential equations and possibly new forms of mathematics will be required to integrate the K-sets into an organic whole.

Table A2.1. Comparison of six methods for measuring phase gradients

This example is from one subject, the other five subjects gave similar findings.

Method	frequency	gradient	diameter	velocity	distance
Units	Hz	ms/rad	mm	m/s	mm
A. Spatial filter applied to phase surface after temporal filtering and cosine fitting					
1. ^a Phase PSD _t	32.2±7.1	.22±.09	7.1±2.9	1.05±0.06	2.2±1.6
2. ^b Wavelets	37.1±8.3	.12±.07	14.7±3.4	1.90±1.13	4.5±2.2
3. ^c Cosines	22.3±6.9	.21±.08	8.6±3.3	0.77±0.40	1.6±0.6
B. Spatial filter applied to EEG before temporal filtering and cosine fitting					
4. ^c FFT	28.2±6.1	.13±.07	14.6±6.8	1.68±0.92	3.2±1.6
5. ^d Hilbert	33.7±7.6	.19±.08	10.2±5.0	1.36±0.72	2.7±2.0
6. ^e AP, APdiff	32.7±7.2	.16±.06	11.3±5.0	1.48±1.24	2.6±1.6

^aFrom the phase spectrum given by the FFT (Freeman and Barrie, 2000)

^bFrom nonlinear regression of AM-FM wavelet decomposition (Freeman, 2003b)

^cPresent study, test case for this purpose

^dSee Tables 1 and 2 for detailed comparisons of the results of Methods 4 and 5.

^eSee Appendix 1.3 in Part 1 for the definition of the analytic phase and sequential differences.

Qualification for phase cones was by spatial SD_x of P_j(t) < .5 rad and spatial SD_x of ΔP_j(t) < 0.1 rad (see Symbol Table 1 in Part 1).

Table A2.2. Effect of varying threshold of % cone residuals for qualifying cones.

Estimates of the temporal wavelength, W_t, and spatial wavelength, W_x, were not significantly affected by changing the threshold criteria of % threshold despite dramatic changes in the numbers and intervals of phase cones. Window duration was 80 ms.

Threshold	counts	intervals	durations	W _t	log W _x
%	N/s	ms	ms	ms/rad	mm/rad
20	5.2	184±210	87.3±13.1	5.01±.97	.77±.19
30	12.3	69.4±68.6	88.3±14.0	4.95±1.01	.77±.19
40	25.6	38.9±36.2	88.6±14.4	4.95±1.07	.79±.20
50	36.2	27.5±23.6	85.2±14.8	4.97±1.12	.80±.22
100	57.8	17.2±12.0	82.1±15.2	4.90±1.15	.78±.25